DOI: 10.1002/ ((please add manuscript number))
Full Paper

Ultrafine Alloy Nanoparticles Converted from Two-Dimensional Intercalated Coordination Polymers for Catalytic Application

*Ping Li, Wen Liu, John S. Dennis, and Hua Chun Zeng**

Dr. P. Li, Prof. H. C. Zeng
Department of Chemical and Biomolecular Engineering
National University of Singapore
119260, Singapore
E-mail: chezhc@nus.edu.sg
Dr. W. Liu, Prof. J. S. Dennis
Department of Chemical Engineering and Biotechnology
University of Cambridge
CB2 3RA, United Kingdom

Keywords: layered double hydroxide, intercalation chemistry, coordination polymer, alloy nanoparticle, cross coupling reaction

Abstract: Supported multimetallic alloy nanoparticles (NPs) have shown great potential for applications owing to combined functions of constituent metals, and more remarkably, enhanced physicochemical properties and even novel synergistic effects that are not possessed by their parent metals. Nevertheless, synthesizing this kind of nanocomposites has been a long-standing challenge using conventional wet chemistry. Herein, we report an efficient, versatile strategy for the preparation of multimetallic alloy NPs supported by layered double hydroxides (LDH) and/or layered double oxides (LDO). In this approach, different metal precursors are intercalated stepwise into the gallery space of LDH. Along with the coordination reaction between the metal precursors, two-dimensional (2D) cyanide bridged coordination polymers (CP) are formed in the confined space. Afterward, supported multimetallic alloy NPs can be obtained *via* either liquid phase reduction or thermal autoreduction. Due to the homogeneous mixing of metals in the 2D CP, ultrafine alloy NPs

can be obtained with high particulate uniformity and compositional tailorability. A large series of supported binary alloy NPs (FePd, FePt, CoPd, CoPt, NiPd, NiPt and PtPd) and ternary alloy NPs (FePdPt, FeNiPt, FeCoPt and NiCoPt) are successfully synthesized with this approach. The resulting supported multimetallic alloy NPs present great potential in numerous applications. To demonstrate their workability, one class of LDH/NiPd nanocomposite is explored as a model heterogeneous catalyst with respect to the carbon-carbon cross coupling reactions (Suzuki-Miyaura, Heck and Sonogashira cross-coupling reactions).

1. Introduction

Metal nanoparticles (NPs), owing to their characteristic surface effect and quantum size effect, display remarkable chemical, optical, electronic, and magnetic properties that are often quite different from their conventional, bulk counterparts.[1] Among them, multimetallic NPs, which are composed of two or more different metal elements, are a large subfamily and have raised intense research attention in recent years.[2] Multimetallic NPs usually display a combination of properties that associate with their constituent metals. More interestingly, in many cases, due to synergistic effect of constituent metal species, they can exhibit enhanced physical and chemical properties and even new properties that do not possess in their respective parental metal species.[3]

To reduce the instability of metal NPs originated from their small size and high surface energy, and to gain better applicability in their practical use, metal NPs are often immobilized on solid supports to prevent them from agglomeration *via* the interaction between the NPs and support.[4] In recent years, many approaches have been developed for the synthesis of supported monometallic NPs, especially for noble metals such Au, Ag, Pd, Pt, etc.[5] However, controllable synthesis of supported alloy NPs, which is much more complicated, is difficult to achieve and only gets limited success.[6] Normally, supported

multimetallic NPs are prepared through conventional impregnation-reduction method, sol-gel processes, or self-assembly between pre-synthesized NPs and a support. Nevertheless, the procedures involved are often complex and time-consuming. Besides, it is not an easy task to simultaneously control the nucleation and growth of two or more distinct metals due to their different thermodynamic and kinetic characteristics under the same synthetic condition. As a result, alloy inhomogeneity is usually unavoidable for the traditional wet chemistry synthesis of supported multimetallic NPs.[7] From the perspective of advancement of metal nanostructures for practical applications such as catalysis, it is highly desirable to develop facile, controllable and efficient routes for the synthesis of multimetallic NPs with homogeneous mixing of constituent metal species on common catalyst supports or carriers.

Concerning potential catalyst supports, layered double hydroxides (LDH) are a class of anionic clay compounds, consisting of positively charged two-dimensional (2D) brucite (*i.e.*, $Mg(OH)_2$) type layers, and exchangeable anions situated in the interlayer space (*i.e.*, gallery space). The general chemical formula of LDH can be written as $[M^{2+}_{1-x}M^{3+}_{x}(OH)_2]^{x+}A^{z-}_{x/z}\cdot mH_2O$, where M^{2+}, M^{3+} and A^{z-} represent di- and trivalent metal cations, and the interlayer anions, respectively.[8] LDH, due to flexibility of compositional tailoring in both brucite-like layers and interlayer anions, together with their unique physicochemical properties, such as ion-exchange ability, surface adsorption capacity and the memory effect, have attracted huge attention in the fields of catalysis,[9] gas adsorption/storage,[10] and energy storage/conversion.[11]

In searching for metal precursors, coordination polymers (CP), which are composed of metal ions (or clusters) and organic linkers, are a type of versatile functional materials.[12] In particular, cyanide bridged transition metal CP exhibit a wide range of properties useful for magnetic, electrical, optical, gas storage and catalytic applications.[13] Among this large subclass of CP, crystalline Prussian Blue and its analogues have been extensively studied in

the past decades.[14] In recent years, furthermore, amorphous cyanide bridged CP, which are fundamentally different from the crystalline CP, have also earned lots of interests.[15] Amorphous cyanide-containing transition metal CP can be generated *via* the reaction between cyanometalate $[M^A(CN)_n]^{2-/3-}$ (n = 4 or 6, M^A = Fe, Co, Ni, Pd, Ru, Os and Cr) and chlorometalate $[M^BCl_4]^{2-}$ (M^B = Pd and Pt).[15a, 15b] During reaction process, two *trans* chloride ligands on the chlorometalate are substituted by the cyanide ligands on the cyanometalate, resulting in the formation of negatively charged, cyanide linked CP (Equation 1).

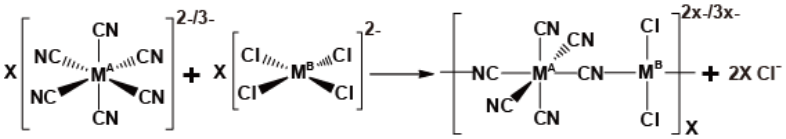

(1)

Herein, we report a novel, facile and effective route for the preparation of supported multimetallic alloy NPs composites by the combination of unique properties of LDH and cyanide bridged CP. In our synthesis, different metal precursors (*i.e.*, cyanometalates and chlorometalates) are intercalated stepwise into the gallery space of LDH, and thus 2D amorphous cyanide bridged transition metal CP are generated *in-situ* through combination of intercalation chemistry and coordination chemistry. After either liquid-phase reduction or thermal autoreduction, the 2D CP confined in the gallery space are converted to ultrafine multimetallic alloy NPs on the support of LDH or LDO.

This strategy holds the following important process advantages: (i) Because of the homogeneous mixing of the transition metal species at an atomic level, the cyanide based CP can readily serve as desirable metal precursors to produce homogeneous multimetallic alloys.[16] (ii) Three-dimensional (3D) hierarchical architecture of flowerlike LDH with designed mesoporosity and surface property facilitate the fabrication of supported multimetallic alloy NPs with extremely small size (about 2 nm) and homogeneous surface

distribution. (iii) Owing to selectable component combinations of metal precursors for cyanide-containing CP, the synthetic reaction is versatile to produce supported alloy NPs with tunable compositions. In this work, a wide variety of binary alloy NPs (FePd, FePt, NiPd, NiPt, CoPd, CoPt and PtPd) and even ternary alloy NPs (FePdPt, FeNiPt, FeCoPt and NiCoPt) are successfully immobilized on the MgAl-LDH/LDO supports. The resulting nanocomposites can be utilized in a wide range of fields, for instance, general heterogeneous catalysis. To demonstrate their effectiveness in this field, we have explored the catalytic activity for various carbon-carbon cross-coupling reactions (*i.e.*, Suzuki-Miyaura, Heck, and Sonogashira cross-couplings) using one class of LDH/NiPd nanohybrid.

2. Results and Discussion

2.1. Overall synthetic strategy

The overall synthesis procedure to produce LDH/LDO-supported multimetallic alloy NPs is schematically presented in **Scheme 1** and described in the Experimental Section in detail. Firstly, uniform 3D flowerlike hierarchical-structured MgAl-LDH spheres were fabricated *via* a one-pot solvothermal method by using metal chlorides as metal precursors, urea as base and methanol as solvent. Then metal-containing anions such as cyanometalate $[M^{A}(CN)_{n}]^{2-/3-}$ (n = 4 or 6) and chlorometalate $[M^{B}Cl_{4}]^{2-}$ were intercalated stepwise into the interlayer space of MgAl-LDH support through ion-exchange with the anions originally located in the gallery of the pristine MgAl-LDH. During such intercalation, polymerization also took place through substitution of two chloride ligands on the chlorometalate by two cyanide groups of the cyanometalate (Equation 1), and thus 2D confined amorphous Prussian-Blue-like cyanide bridged transition metal CP was generated in the gallery space of LDH, giving rise to the intermediate product LDH/$M^{A}M^{B}$ CP. In this type of 2D transition metal CP, different metal species were homogeneously mixed at an atomic level, and the close connection among metal species would greatly facilitate the generation of alloy clusters combined from different metal

atoms nearby upon their reduction. Finally, after either liquid-phase reduction by $NaBH_4$ or thermal autoreduction under inert atmosphere, LDH/M^AM^B CP was converted to LDH/LDO-supported multimetallic alloy NPs (*i.e.*, LDH/M^AM^B and LDO/M^AM^B) with uniform NPs highly dispersed on the support matrices.

2.2. Hierarchical structured flowerlike MgAl-LDH

MgAl-LDH support used in this work was fabricated *via* a simple one-pot solvothermal method. SEM and TEM images (**Figure 1**a, b and S1a) show that the as-synthesized MgAl-LDH is uniform flowerlike particles which are formed by a large number of thin petals connecting with each other. Their diameter is in the range of 2-3 μm and the thickness of nanosheet building blocks is only about 10 nm. X-ray diffraction (XRD) pattern of MgAl-LDH (Figure 1c) indicates the characteristic reflections of a typical hydrotalcite-like phase with a series of symmetric (*00l*) peaks which can be indexed to a hexagonal lattice with a rhombohedral symmetry (*R*-3*m*). On the basis of the (003) diffraction peak, the interlayer distance of MgAl-LDH is calculated to be 0.78 nm. Besides, the Debye-Scherrer equation is applied to estimate the thickness of MgAl-LDH nanosheet building blocks by using the (003) as well as (006) diffraction peaks, and the average thickness is calculated to be ca. 12 nm. Figure 1d shows the FTIR spectrum of MgAl-LDH. The strong, broad peaks at around 3450 cm^{-1} and 1600 cm^{-1} are associated with the interlayer water molecules. The bands around 2950 cm^{-1}, 2850 cm^{-1}, 1450 cm^{-1}, 1380 cm^{-1} and 1060 cm^{-1} are assigned to the stretching, bending vibrations of C–H and stretching vibration of C–O from the intercalated methoxide anions in the interlayer of MgAl-LDH, respectively.[17] The EDX analysis (Figure S1b) confirms its chemical compositions and demonstrates the presence of Cl element, which originates from the intercalated Cl^- in the gallery space of LDH. The atomic ratio of Mg/Al in the MgAl-LDH is 2.07 determined from ICP-AES analysis. Nitrogen adsorption/desorption measurement (Figure S2) of the pristine MgAl-LDH shows a type IV isotherm with H3

hysteresis loop, indicating the presence of mesoporous structure. The specific BET surface area is 93.9 m^2/g. All these features (3D hierarchical architecture, large surface area, and mesoporous nanostructure) make MgAl-LDH an excellent catalyst support.

2.3. M^AM^B CP formed in the gallery space of LDH

The approach described in Scheme 1 is remarkably versatile. Because of abundant choices of cyanometalates and chlorometalates, 2D amorphous cyanide-containing CP with different chemical compositions can be intercalated in the MgAl-LDH host. Firstly in this work, we have prepared a range of binary metallic CP, namely, FePd CP, FePt CP, CoPd CP, CoPt CP, NiPd CP, NiPt CP and PtPd CP confined within the 2D gallery space of LDH.

As shown in the SEM and TEM images (Figure S3 and S4), for all the LDH/M^AM^B CP, the flowerlike morphology of the LDH host is well preserved after the intercalation of cyanide bridged CP. Because the 2D CP are formed in the gallery space of LDH through ion-exchange (Equation 1), no noticeable morphological changes are observed in these TEM images when compared with the pristine MgAl-LDH. However, EDX analysis (Figure S5) confirms that all the LDH/M^AM^B CP contain corresponding metal elements.

To shed light on the formation mechanism, the synthesis process of LDH/M^AM^B CP and the nature of the intercalated moieties in each step were investigated with both FTIR and XRD techniques. In the FTIR spectra of LDH/$[M^A(CN)_n]^{2-/3-}$ (**Figure 2**a-d), new bands appear in the spectral window of 2000-2200 cm^{-1} which can be assigned to stretching vibration modes of cyano group, in addition to those associated with the pristine MgAl-LDH host. The presence of these new bands verifies the successful intercalation of $[M^A(CN)_n]^{2-/3-}$ species in the LDH host. After the secondary intercalation of $[M^BCl_4]^{2-}$, LDH/M^AM^B CP are obtained. Compared with that of LDH/$[M^A(CN)_n]^{2-/3-}$, the variation in the wavenumber of the cyanide vibration modes and/or the change in its multiplicity indicate the formation of coordination bonds in the LDH/M^AM^B CP.

Figure 2e-h display the XRD patterns of LDH/$[M^A(CN)_n]^{2-/3-}$ and LDH/M^AM^B CP. All of them exhibit a typical pristine LDH pattern with well-defined peaks, revealing good retention of crystallinity of the LDH phase even after the formation of nanohybrids. Meanwhile, noticeable evolutions, that is, a new set of (*00l*) diffraction peaks emerging at lower 2θ angles are observed, which are associated with an increase of the basal spacing of the original LDH owing to successful intercalation of $[M^A(CN)_n]^{2-/3-}$ and M^AM^B CP in the gallery space. Because the original LDH in these nanohybrids is still present, it is understood that there is still room for further intercalation in the LDH host. Apart from the expansion of inter-brucite-sheet distance, due to the amorphous nature of 2D M^AM^B CP, no diffraction peaks indexed to a bulk phase CP display in the XRD patterns of LDH/M^AM^B CP.

As for the XRD pattern of LDH/PtPd CP (Figure 2h), it is worth noting that the intensity of the peak around $2\theta = 18°$, which is assigned to the (006) reflection of the intercalated LDH, is remarkably intensive. Obviously, this peak is much more intense than that of the (003) reflection of the same intercalated LDH. Similar phenomenon has been reported previously and it can be attributed to the increase of the electronic density in the interlayer space resulting from the presence of the heavy metal Pt and Pd-containing species in the LDH gallery.[18]

2.4. Fabrication of LDH/M^AM^B nanocomposites

A series of LDH supported binary alloy NPs (LDH/M^AM^B, M^AM^B = FePd, FePt, CoPd, CoPt, NiPd, NiPt and PtPd**)** can be prepared *via* conversion of the above LDH/M^AM^B CP upon the addition of reducing agent $NaBH_4$. All the obtained LDH/M^AM^B nanocomposites were systematically characterized by SEM, TEM, EDX elemental mapping and XRD, and the results are listed in Supporting Information.

In the case of LDH/NiPd, for example, the SEM and TEM images (**Figure 3**a, b) reveal that the original flowerlike morphology of the precursor (LDH/NiPd CP) is still maintained.

High magnification TEM images (Figure 3c, d) show that uniform, tiny NiPd alloy NPs (about 2 nm in size) are monodispersed on the surface of the MgAl-LDH petals. EDX elemental mapping (Figure 3e) demonstrates that the sample indeed contains nickel, palladium apart from aluminum and magnesium, which is in good agreement with the chemical composition of LDH/NiPd. In the FTIR spectrum of LDH/NiPd (Figure 3f), characteristic stretching mode of cyanide ligand (2133 cm^{-1}) is no longer observable, indicating a complete transformation of NiPd CP to the metallic alloy (NiPd). In addition, no diffraction peaks indicative of the metallic Ni, Pd or NiPd phase are detectable in the XRD pattern (Figure 3g), which can be ascribed to the extremely small size and high dispersion of NiPd NPs on the LDH support, in good agreement with the TEM result (Figure 3b-d). Besides, nitrogen sorption measurement of LDH/NiPd shows that the nanocomposite can still retain large BET specific surface area (81.5 m^2/g; Figure S6).

LDH-supported binary alloy NPs of noble metal alloy, LDH/PtPd, has also been fabricated with the same synthetic approach using Na_2PdCl_4 and $K_2Pt(CN)_4$ as precursors. The SEM and TEM images (**Figure 4**a-d) show that monodispersed PtPd alloy NPs (about 2 nm in size) are also distributed evenly on the petals of the MgAl-LDH support. EDX elemental mapping (Figure 4e) confirms the chemical composition of LDH/PtPd. No characteristic stretching vibrations of cyanide (2205 and 2145 cm^{-1}) are identifiable from the FTIR spectrum (Figure 4f). Furthermore, owing to the extremely small size and high dispersion of PtPd alloy NPs, no diffraction peaks indexed to mono-metals (Pt or Pd) and alloy phase are found in the XRD pattern (Figure 4g). Similarly, nitrogen sorption measurement also reveals a large BET specific surface area (76.5 m^2/g; Figure S7) for this sample.

For the cases of other supported LDH/M^AM^B nanocomposites (LDH/FePd, LDH/FePt, LDH/CoPd, LDH/CoPt and LDH/NiPt), similar characterization results are observed and they are reported in Supporting Information (see Figure S8-S12 for SEM, TEM and EDX

elemental mapping; Figure S13 for XRD; and Table S3 for chemical compositions of these samples determined from ICP-AES analysis). All these LDH/M^AM^B samples inherit the original hierarchical structure of the MgAl-LDH support and uniform binary alloy NPs (about 2 nm in size) are evenly distributed on the petals of the flowerlike LDH.

2.5. Autoreduction as an alternative route for LDO-supported multimetallic alloy NPs

The autoreduction chemistry of cyanide bridged transition metal CP is quite intriguing and noteworthy. The cyanide ligands in the polymeric materials can serve as a reducing agent and convert the transition metal ions to the lower oxidation state at elevated temperature under an inert atmosphere.[16a, 19] This desirable autoreduction feature can be utilized in alloy NPs preparation.

Considering this peculiar property of cyanide containing CP, the conversion of the intermediate samples of LDH/M^AM^B CP to the supported multimetallic alloy NPs can be also achieved through thermal autoreduction, in addition to using $NaBH_4$. For example, without any additional reducing agent, LDO/NiPd, LDO/CoPd and LDO/PtPd could be prepared by heating their solid precursors LDH/NiPdCP, LDH/CoPdCP and LDH/PtPdCP at 600 °C, 600 °C and 450 °C for 100 min under Ar atmosphere, respectively. As shown in SEM (Figure S14) and TEM images (**Figure 5**), once again, the product alloy NPs are quite uniform with narrow particle size distribution (5-7 nm for NiPd NPs, 3-5 nm for CoPd NPs and 1-3 nm for PtPd NPs) and highly dispersed on the surface of support with well-kept flowerlike morphology after autoreduction. In the XRD patterns of these LDO-supported alloy NPs (Figure 5c, f, i), the original LDH phase disappears and two new peaks (at 2θ = 42.9° and 62.3°) emerge, which can be indexed to cubic phase MgO (JCPDF card no. 45-0946), verifying the conversion of LDH to LDO during heat treatment.

For the XRD pattern of LDO/NiPd (Figure 5c), no diffraction peaks assigned to single-component Ni or Pd metal are observed. Besides, it is noted that the diffraction peaks of NiPd

species shift towards higher angle relative to the peaks of Pd (JCPDS no. 05-0681), further demonstrating the formation of NiPd alloy. Similarly, XRD patterns of LDO/CoPd (Figure 5f) and LDO/PtPd (Figure 5i) indicate the formation of homogeneous CoPd alloy and PtPd alloy with no segregation of monometallic phase.

2.6. Versatility of this approach

Apart from the above supported binary alloy nanocomposites, similarly, ternary alloy NPs can also be synthesized on the LDH support using three different chlorometalates and cyanometalates at the same time. As a proof-of-concept study, in this work, a series of ternary alloy NPs (FeCoPt, FePdPt, FeNiPt and NiCoPt) have been successfully prepared on the MgAl-LDH support, highlighting the versatility and reproducibility of this synthetic strategy.

Characterizations of the above LDH-supported multimetallic alloy NPs including SEM, TEM, EDX elemental mapping, XRD and ICP-AES analysis are detailed in **Figure 6**, Figure S15-S18 and Table S4. As can be seen, the original flowerlike morphology of LDH support is reserved well for all these samples (Figure 6 and S15-S17). Impressively, all alloy NPs are uniform with particle size ranging from 2 to 3 nm and evenly dispersed on the surface of support. Moreover, the EDX elemental mappings further confirm the chemical compositions of the nanocomposites. Similar to their binary counterparts, XRD patterns (Figure S18) of these samples exhibit characteristic peaks corresponding to the pristine LDH phase as well as those indexed to the intercalated LDH, while no peaks assigned to individual metal or alloy phase are observed because of the extremely small size and high dispersion of alloy NPs on the LDH support. In addition, based on the above characterizations, we propose a plausible formation mechanism of LDH/M^AM^B nanocomposites from the LDH/M^AM^B CP precursors, as illustrated in Scheme S1.

2.7. Catalytic performance of LDH/M^AM^B

Owing to the 3D hierarchical architecture and mesoporous nanostructure of LDH/LDO support, coupled with the extremely small size and remarkably high dispersion of alloy NPs

on the support, the above LDH/LDO-supported multimetallic alloy NPs are expected to hold promising potential in the field of catalysis. In this work, we select carbon-carbon cross-coupling reactions for catalyst evaluation. It is well known that Suzuki-Miyaura, Heck and Sonogashira cross-coupling reactions are one of the most efficient pathways for the carbon-carbon bond formation and they are frequently exploited in modern synthetic chemistry.[20] In particular, Pd-based catalysts, either homogeneous palladium-based complexes or heterogeneous ones, are commonly used in these reactions.[21] Herein we choose one class of the above supported binary alloy NPs, LDH/NiPd (Pd: 3.82 wt%, Ni: 1.14 wt%, Ni/Pd = 1/2) for this activity evaluation in view of its low-cost metal combination (*i.e.*, Ni is much cheaper than Pd).

The catalytic performance of LDH/NiPd was firstly investigated in the Suzuki-Miyaura cross-coupling reaction between iodobenzene and phenylboronic acid. Catalytic properties of a number of control samples were also investigated for comparison and the results are summarized in **Figure 7**. In the case of LDH/Ni, the cross-coupling reaction could not proceed since nickel is not an active catalyst for this reaction. For the LDH-supported monometallic NPs, LDH/Pd, the yield reached 85 % in 30 min. When using the LDH/NiPd composite, the reaction proceeded smoothly with 97.0% yield in 30 min, suggesting the advantage of alloy NPs compared with the single component metallic NPs. We propose that the superiority of LDH/NiPd composite can be attributed to the synergistic effect between Ni and Pd species in the alloy. As for Pd-catalyzed carbon-carbon cross-coupling reaction, the oxidative addition of aryl halide to the Pd is the key elementary step, and the enhancement of electron density of Pd species can promote the oxidative addition step and thus enhance reaction rate.[22] In our case of LDH/NiPd, the intimate contact between Ni and Pd in the alloy and their different electronegativity lead to a significant increase in electron density of Pd atoms, and thus facilitate the oxidative addition of aryl halide to the Pd surface, resulting in higher activity than the single component metallic Pd NPs (*i.e.*, LDH/Pd).

To find a wider scope of application, a class of other reaction substrates was also tested, as listed in **Table 1**. In the presence of LDH/NiPd, aryl iodides with either electron-withdrawing substituent (–$COCH_3$, –NO_2) or electron-donating substituent (–OCH_3, –OCH_3) showed 96.5–100% yields for the corresponding biaryl products after reaction time of 15-30 min (Table 1, entries 1-5). For bromobenzene and aryl bromide with different substituted groups such as –$COCH_3$, the reaction can proceed and give modest to good yields of the corresponding products within 1-3 h (Table 1, entries 6-7).

In addition, LDH/NiPd composite was also used to perform other types of cross-coupling reactions. In the case of Heck cross-coupling reaction between iodobenzene and methyl acrylate (Equation 2), an excellent yield of 100% could be achieved after 1 h. For the Sonogashira cross-coupling reaction between iodobenzene and phenylacetylene (Equation 3), a satisfactory yield of 95% could also be obtained after reaction time of 1 h in the presence of LDH/NiPd.

(2)

(3)

Moreover, we have compared the performance of LDH/NiPd composite in this work with those of other Pd-based catalysts reported in the literature. As shown in Table S5, the corresponding turnover frequency (TOF) for our LDH/NiPd composite in the coupling reaction between iodobenzene and phenylboronic acid is calculated to be 462 h^{-1}. This value is much higher than that of many other reported Pd-based catalysts under similar reaction conditions, demonstrating the excellent performance of our catalysts. All these results illustrate that due to the large surface area and hierarchical structure of MgAl-LDH support, the synergistic effect between Ni and Pd species, together with high monodispersity of tiny

alloy NPs, LDH/NiPd composite is able to serve as an efficient nanocatalyst for Pd-catalyzed organic transformations.

For catalysis, stability and recycling ability of catalyst is another critical application criterion. The recyclability of LDH/NiPd was evaluated in the Suzuki–Miyaura cross-coupling reaction between iodobenzene and phenylboronic acid. After each cycle of the reaction, the solid catalyst was retrieved by centrifugation, washed with water/ethanol and then reused in the next consecutive run. Quite encouragingly, our LDH/NiPd could be recycled up to 6 times with negligible loss in catalytic activity over the continuous catalytic cycles (**Figure 8**a). ICP-AES analysis of LDH/NiPd after being reused for 6 times reveals that there is no appreciable change in Pd loading (97.7 % Pd remained in the used catalyst). In addition, SEM and TEM studies of the used LDH/NiPd sample show that the flowerlike morphology of LDH support is maintained well, and NiPd NPs are still immobilized on the surface of support (Figure 8b, c). We propose that the excellent stability of LDH/NiPd composite can be ascribed to the special structural features of the nanocatalyst. The 3D hierarchical-structured LDH with abundant surface hydroxyl groups can act as an excellent support, which not only disperse alloy NPs, but also effectively suppress their leaching and aggregation during application, and thus improve their stability. In addition, the concave surface topology of flowerlike LDH can also prevent the supported metal NPs from mutual collision, thus the detachment of metal can be minimized.

3. Conclusion

In summary, we have developed an efficient and versatile approach for the fabrication of supported multimetallic alloy NPs. With this synthetic route, chlorometalate and cyanometalate anions are intercalated sequentially into the interlayer space of MgAl-LDH support, leading to formation of 2D cyanide bridged transition metal coordination polymers (CP) through the coordination reaction. Afterward, the confined 2D CP can be converted to

alloy NPs *via* liquid phase reduction or thermal autoreduction, producing LDH/LDO-supported multimetallic alloy nanocomposites. A wide variety of ultrafine multicomponent alloy NPs, including binary alloy NPs (FePd, FePt, CoPd, CoPt, NiPd, NiPt and PtPd) and ternary alloy NPs (FePdPt, FeNiPt, FeCoPt and NiCoPt) are successfully loaded onto the LDH/LDO support with high dispersion. Among these supported alloy nanocomposites, one class of LDH/NiPd nanohybrid is evaluated as a catalyst to perform various carbon-carbon cross-coupling reactions, which exhibits excellent activity, selectivity and reusability owing to the special physicochemical structural features of the nanocatalyst such as highly-dispersed ultrafine alloy NPs and unique architecture. We believe the findings from the combination of intercalation chemistry and coordination chemistry in this work are important for future design and synthesis of alloy nanostructures with various compositions and functions.

4. Experimental Section

4.1. Materials and reagents. The following chemicals were used as received without further purification. $MgCl_2 \cdot 6H_2O$ (99+%, Sigma-Aldrich), $AlCl_3 \cdot 6H_2O$ (99+%, Sigma-Aldrich), urea (99.5%, Fluka), methanol (99.99%, Fisher), ethanol (99.99%, Fisher), *N*,*N*-dimethylformamide (DMF, 99.99%, Fisher), sodium borohydride (99.99%, Sigma-Aldrich), palladium (II) chloride (99.9%, Sigma-Aldrich), potassium tetrachloroplatinate (II) (99%, Sigma-Aldrich), sodium chloride (99%, Sigma-Aldrich), potassium carbonate (99%, Sigma-Aldrich), methyl acrylate (99.9%, Fisher), aryl halides (98-99.5%, Sigma-Aldrich), phenylboronic acid (98%, Sigma-Aldrich), phenylacetylene (98%, Sigma-Aldrich), potassium hexacyanoferrate (III) ($K_3[Fe(CN)_6]$, 98+%, Sigma-Aldrich), potassium hexacyanocobalt (III) ($K_3[Co(CN)_6]$, 97%, Sigma-Aldrich), potassium tetracyanoplatinate (II) ($K_2[Pt(CN)_4]$, 98%, Sigma-Aldrich), and potassium tetracyanonickelate (II) hydrate ($K_2[Ni(CN)_4] \cdot xH_2O$, 99%, Sigma-Aldrich). Deionized water was collected through the Elga Micromeg Purified Water system.

4.2. Preparation of flowerlike MgAl-LDH spheres. Flowerlike MgAl-LDH spheres was synthesized by previously reported method with minor modifications.[9a] In a typical synthesis, briefly, $MgCl_2 \cdot 6H_2O$, $AlCl_3 \cdot 6H_2O$ and urea with a molar ratio of 3:1:7 were dissolved in 30 mL of methanol. The above mixture was stirred and then transferred into a Teflon-lined autoclave, sealed and heated at 150 °C for 10 h. The product was centrifuged, rinsed with deionized water and ethanol for several times and dried in an electric oven at 70 °C for 12 h.

4.3. Preparation of cyanide bridged CP (M^AM^B CP and $M^AM^BM^C$ CP) in the gallery space of MgAl-LDH. Different LDH/M^AM^B CP were synthesized through the stepwise intercalation of cyanometalate $[M^A(CN)_n]^{2-/3-}$ (n = 4 or 6) and chlorometalate $[M^BCl_4]^{2-}$ into the interlayer space of MgAl-LDH. In a typical synthesis, the above obtained flowerlike MgAl-LDH spheres were dispersed in 30 mL of deionized water containing $[M^A(CN)_n]^{2-/3-}$ and stirred for 3 h, then a certain amount of $[M^BCl_4]^{2-}$ aqueous solution was added and stirred for another 3 h. In this way, 2D M^AM^B CP were formed inside the confined space of LDH (Equation 1), producing LDH/M^AM^B CP.

Different types of LDH/M^AM^B CP or LDH/$M^AM^BM^C$ CP were synthesized by following the same preparative procedure while using different metal precursor combinations (*i.e.*, different chlorometalates and cyanometalates). More specifically, in the cases of LDH/binary metallic CP, $K_3[Fe(CN)_6]$ and Na_2PdCl_4 for LDH/FePd CP; $K_3[Fe(CN)_6]$ and K_2PtCl_4 for LDH/FePt CP; $K_2[Ni(CN)_4]$ and Na_2PdCl_4 for LDH/NiPd CP; $K_2[Ni(CN)_4]$ and K_2PtCl_4 for LDH/NiPt CP; $K_3[Co(CN)_6]$ and Na_2PdCl_4 for LDH/CoPd CP; $K_3[Co(CN)_6]$ and K_2PtCl_4 for LDH/CoPt CP; and $K_2[Pt(CN)_4]$ and Na_2PdCl_4 for LDH/PtPd CP were used in their respective synthesis. In the cases of LDH/ternary metallic CP, moreover, $K_3[Fe(CN)_6]$, K_2PtCl_4 and Na_2PdCl_4 for LDH/FePdPt CP; $K_3[Fe(CN)_6]$, $K_2[Ni(CN)_4]$ and K_2PtCl_4 for LDH/FeNiPt CP; $K_3[Fe(CN)_6]$, $K_3[Co(CN)_6]$ and K_2PtCl_4 for LDH/FeCoPt CP; $K_2[Ni(CN)_4]$, $K_3[Co(CN)_6]$ and K_2PtCl_4 for

LDH/NiCoPt CP were used in their respective synthesis. The experimental details on the amounts of different metal precursors used were listed in Table S1 and S2.

4.4. Preparation of LDH-supported multimetallic NPs (LDH/M^AM^B and LDH/$M^AM^BM^C$). The conversion of LDH/M^AM^B CP or LDH/$M^AM^BM^C$ CP to LDH/M^AM^B or LDH/$M^AM^BM^C$ was achieved *via* a simple liquid-phase reduction method with $NaBH_4$ as a reducing agent. Briefly, the above obtained LDH/M^AM^B CP or LDH/ $M^AM^BM^C$ CP were redispersed in 30 mL of deionized water. Then freshly prepared aqueous solution of $NaBH_4$ (20 mM) was added into the suspension and the resultant reaction mixture was stirred for 1 h to ensure the complete reduction of metal ions. The final products were collected, washed with deionized water and ethanol in sequence, and dried at 50 °C overnight.

4.5. Preparation of LDH-supported monometallic NPs (for control experiments). Preparation of LDH/Pd: Briefly, flowerlike MgAl-LDH spheres (100 mg) were dispersed in 30 mL of deionized water containing a certain amount of Na_2PdCl_4 and stirred for 3 h. The product was collected by centrifugation, washed with water and redispersed in 30 mL of deionized water. Then a freshly prepared aqueous solution of $NaBH_4$ (20 mM) was added and stirred for another 1 h to ensure the complete reduction of Pd^{2+} ions. The final product was collected, washed with deionized water and ethanol in sequence, and dried at 50 °C overnight.

Preparation of LDH/Ni: LDH/Ni was synthesized using the same preparation method for the above LDH/Pd, except for replacing Na_2PdCl_4 with a nickel salt $NiCl_2$.

4.6. Preparation of LDO-supported multimetallic NPs via an autoreduction route. Instead of reductant $NaBH_4$, the cyanide based transition metal CP can also be converted to their corresponding alloy NPs *via* thermal autoreduction by using cyanide groups in the polymer as the reducing agent.

In the following, we take the preparations of LDO/NiPd, LDO/CoPd and LDO/PtPd samples to highlight the main process steps. The LDO/NiPd was prepared by thermolysis of

LDH/NiPd CP at 600 °C under an Ar atmosphere for 100 min with a heating rate of 2 °C/min; the LDO/CoPd was obtained by thermolysis of LDH/CoPd CP at 600 °C under Ar atmosphere for 100 min at a heating rate of 2 °C/min; and the LDO/PtPd was prepared by heating LDH/PtPd CP at 450 °C under the same Ar atmosphere for 100 min with a ramping rate of 2 °C/min.

4.7. Catalytic activity evaluation. Suzuki-Miyaura cross-coupling reaction: Ethanol (10 mL), aryl halide (0.5 mmol), aryl boronic acid (1 mmol), *n*-dodecane (0.5 mmol, as an internal standard for GC), K_2CO_3 (2 mmol) were placed in a glass reactor and heated to 80 °C. Then solid catalyst LDH/NiPd (0.42 mol% Pd in reaction system, atomic ratio of Ni/Pd = 1/2) was added. The resulting mixture was stirred at 80 °C under ambient atmosphere for a given time. The reaction was stopped by cooling the reactor to room temperature. The solid catalyst was then separated *via* centrifugation, and the supernatant was analyzed by gas chromatography (GC, Agilent-7890A) equipped with a capillary column (HP-5, 30.0 m × 320 μm × 0.25 μm) and a flame ion detector (FID). The products were further confirmed by gas chromatography-mass spectrometry (GC-MS, Agilent, 7890A-5975C) with a capillary column (DB-5 ms, 30.0 m × 320 μm × 0.25 μm).

Heck cross-coupling reaction: DMF (10 mL), iodobenzene (0.5 mmol), methyl acrylate (1 mmol), *n*-dodecane (0.5 mmol, as the internal standard), K_2CO_3 (2 mmol) were placed in a glass reactor and heated to 120 °C. Then solid catalyst LDH/NiPd (0.42 mol% Pd in the reaction system, atomic ratio of Ni/Pd = 1/2) was added. The resultant mixture was stirred at 120 °C in ambient atmosphere for a desired time. Then the reaction was stopped by the same cooling to room temperature, followed by the separation of the catalyst LDH/NiPd through centrifuging. The supernatant was analyzed by the GC method, and the products identified were further confirmed by the GC-MS analysis.

Sonogashira cross-coupling reaction: DMF (10 mL), iodobenzene (0.5 mmol), phenylacetylene (1 mmol), *n*-dodecane (0.5 mmol, as the internal standard), K_2CO_3 (2 mmol) were placed in a glass reactor and heated to 120 °C. Then solid catalyst LDH/NiPd (0.42 mol% Pd in the reaction system, atomic ratio of Ni/Pd = 1/2) was added. The prepared mixture was stirred at 120 °C under ambient atmosphere for a given time. The reaction was then stopped by the same cooling process to room temperature. Afterward, the LDH/NiPd catalyst was separated *via* centrifugation, and the supernatant was analyzed by the GC technique. The products were further confirmed by the GC-MS analysis.

4.8. Materials characterization. The microscopic features of the samples were characterized by scanning electron microscopy (SEM, JEOL-6700F) equipped with an energy-dispersive X-ray (EDX) analyzer (Oxford INCA), transmission electron microscopy (TEM, JEOL JEM-2010, 200 kV), and high resolution transmission electron microscopy (HRTEM, JEOL JEM-2100F, 200 kV). The elemental mapping was done by energy-dispersive X-ray spectroscopy (EDX, Oxford Instruments, model 7426). The wide-angle X-ray diffraction patterns were taken on Bruker D8 Advance system (Cu K_α radiation). Nitrogen adsorption–desorption isotherms were obtained at 77 K on a Quantachrome NOVA-3000 system. The surface areas of the studied materials were determined by the Brunauer–Emmet–Teller (BET) method. Inductively coupled plasma (ICP) analysis (Dual-view Optima 5300 DV ICP-OES) was also made to measure the elemental compositions for the above studied samples. Fourier transform infrared spectroscopy (FTIR, Bio-Rad FTS-135) was used to obtain chemical bonding information of samples using the potassium bromide (KBr) pellet technique.

Supporting Information

Supporting Information is available from the Wiley Online Library or from the author.

Acknowledgements

The authors gratefully acknowledge the financial support provided by the Ministry of Education, Singapore, NUS, and GSK Singapore. This project is also funded by the National

Research Foundation (NRF), Prime Minister's Office, Singapore, under its Campus for Research Excellence and Technological Enterprise (CREATE) program.

Received: ((will be filled in by the editorial staff))
Revised: ((will be filled in by the editorial staff))
Published online: ((will be filled in by the editorial staff))

[1] a) M. A. El-Sayed, *Acc. Chem. Res.* **2004**, *37*, 326; b) V. Polshettiwar, R. S. Varma, *Green Chem.* **2010**, *12*, 743; c) L. Wang, Y. Nemoto, Y. Yamauchi, *J. Am. Chem. Soc.* **2011**, *133*, 9674; d) H. Zhang, M. Jin, Y. Xia, *Angew. Chem. Int. Ed.* **2012**, *51*, 7656; e) S. Guo, S. Zhang, S. Sun, *Angew. Chem. Int. Ed.* **2013**, *52*, 8526; f) H. Ataee-Esfahani, M. Imura, Y. Yamauchi, *Angew. Chem. Int. Ed.* **2013**, *52*, 13611; g) C. Li, T. Sato, Y. Yamauchi, *Angew. Chem. Int. Ed.* **2013**, *52*, 8050; h) Y. Zhou, H. C. Zeng, *J. Am. Chem. Soc.* **2014**, *136*, 13805; i) J. Lai, W. Niu, R. Luque, G. Xu, *Nano Today* **2015**, *10*, 240.

[2] a) D. Wang, Y. Li, *Adv. Mater.* **2011**, *23*, 1044; b) A. K. Singh, Q. Xu, *ChemCatChem* **2013**, *5*, 652; c) H.-l. Liu, F. Nosheen, X. Wang, *Chem. Soc. Rev.* **2015**, *44*, 3056.

[3] a) W. Yu, M. D. Porosoff, J. G. Chen, *Chem. Rev.* **2012**, *112*, 5780; b) B. Y. Xia, H. B. Wu, N. Li, Y. Yan, X. W. Lou, X. Wang, *Angew. Chem. Int. Ed.* **2015**, *54*, 3797; c) V. Mazumder, Y. Lee, S. Sun, *Adv. Funct. Mater.* **2010**, *20*, 1224.

[4] a) H. C. Zeng, *Acc. Chem. Res.* **2012**, *46*, 226; b) P. Li, H. Liu, Y. Yu, C.-Y. Cao, W.-G. Song, *Chemistry – An Asian Journal* **2013**, *8*, 2459; c) G. Prieto, J. Zečević, H. Friedrich, K. P. de Jong, P. E. de Jongh, *Nat Mater* **2013**, *12*, 34; d) Y. Sheng, H. C. Zeng, *Chem. Mater.* **2015**, *27*, 658.

[5] a) H. Yin, S. Zhao, K. Zhao, A. Muqsit, H. Tang, L. Chang, H. Zhao, Y. Gao, Z. Tang, *Nat Commun* **2015**, *6*; b) C. Jiang, K. Hara, A. Fukuoka, *Angew. Chem. Int. Ed.* **2013**, *52*, 6265.

[6] a) S. Guo, S. Sun, *J. Am. Chem. Soc.* **2012**, *134*, 2492; b) G. J. Hutchings, C. J. Kiely, *Acc. Chem. Res.* **2013**, *46*, 1759.

[7] B. t. Heinrichs, P. Delhez, J.-P. Schoebrechts, J.-P. Pirard, *J. Catal.* **1997**, *172*, 322.

[8] Q. Wang, D. O'Hare, *Chem. Rev.* **2012**, *112*, 4124.

[9] a) P. Li, P.-P. Huang, F.-F. Wei, Y.-B. Sun, C.-Y. Cao, W.-G. Song, *J. Mater. Chem. A* **2014**, *2*, 12739; b) C. Li, M. Wei, D. G. Evans, X. Duan, *Small* **2014**, *10*, 4469; c) C. P. Chen, P. Gunawan, X. W. Lou, R. Xu, *Adv. Funct. Mater.* **2012**, *22*, 780.

[10] Q. Song, W. Liu, C. D. Bohn, R. N. Harper, E. Sivaniah, S. A. Scott, J. S. Dennis, *Energy Environ. Sci.* **2013**, *6*, 288.

[11] a) F. Song, X. Hu, *Nat Commun* **2014**, *5*; b) P. Vialat, C. Mousty, C. Taviot-Gueho, G. Renaudin, H. Martinez, J. C. Dupin, E. Elkaim, F. Leroux, *Adv. Funct. Mater.* **2014**, *24*, 4831.

[12] a) W. Lin, W. J. Rieter, K. M. L. Taylor, *Angew. Chem. Int. Ed.* **2009**, *48*, 650; b) X. Zhang, W. Wang, Z. Hu, G. Wang, K. Uvdal, *Coord. Chem. Rev.* **2015**, *284*, 206.

[13] M. Hu, A. A. Belik, M. Imura, Y. Yamauchi, *J. Am. Chem. Soc.* **2013**, *135*, 384.

[14] a) S. S. Kaye, J. R. Long, *J. Am. Chem. Soc.* **2005**, *127*, 6506; b) M. Hu, S. Ishihara, Y. Yamauchi, *Angew. Chem. Int. Ed.* **2013**, *52*, 1235.

[15] a) B. W. Pfennig, A. B. Bocarsly, R. K. Prud'homme, *J. Am. Chem. Soc.* **1993**, *115*, 2661; b) R. S. Deshpande, S. L. Sharp-Goldman, J. L. Willson, A. B. Bocarsly, J. Gross, A. C. Finnefrock, S. M. Gruner, *Chem. Mater.* **2003**, *15*, 4239; c) Q. Zhu, P. Wu, J. Zhang, W. Zhang, Y. Zhou, Y. Tang, T. Lu, *ChemSusChem* **2015**, *8*, 131.

[16] a) M. Vondrova, C. M. Burgess, A. B. Bocarsly, *Chem. Mater.* **2007**, *19*, 2203; b) C. M. Burgess, M. Vondrova, A. B. Bocarsly, *J. Mater. Chem.* **2008**, *18*, 3694.

[17] E. Gardner, K. M. Huntoon, T. J. Pinnavaia, *Adv. Mater.* **2001**, *13*, 1263.

[18] a) P. Beaudot, M. E. De Roy, J. P. Besse, *J. Solid State Chem.* **2001**, *161*, 332; b) S. Hamada, K. Ikeue, M. Machida, *Chem. Mater.* **2005**, *17*, 4873.

[19] M. Vondrova, T. M. McQueen, C. M. Burgess, D. M. Ho, A. B. Bocarsly, *J. Am. Chem. Soc.* **2008**, *130*, 5563.

[20] a) J. Magano, J. R. Dunetz, *Chem. Rev.* **2011**, *111*, 2177; b) C. C. C. Johansson Seechurn, M. O. Kitching, T. J. Colacot, V. Snieckus, *Angew. Chem. Int. Ed.* **2012**, *51*, 5062.

[21] a) D. Astruc, *Inorg. Chem.* **2007**, *46*, 1884; b) Á. Molnár, *Chem. Rev.* **2011**, *111*, 2251; c) A. Balanta, C. Godard, C. Claver, *Chem. Soc. Rev.* **2011**, *40*, 4973; d) B. Y. Li, Z. H. Guan, W. Wang, X. J. Yang, J. L. Hu, B. E. Tan, T. Li, *Adv. Mater.* **2012**, *24*, 3390.

[22] G. C. Fu, *Acc. Chem. Res.* **2008**, *41*, 1555.

Scheme 1. Synthesis procedure for LDH/LDO-supported multimetallic alloy NPs.

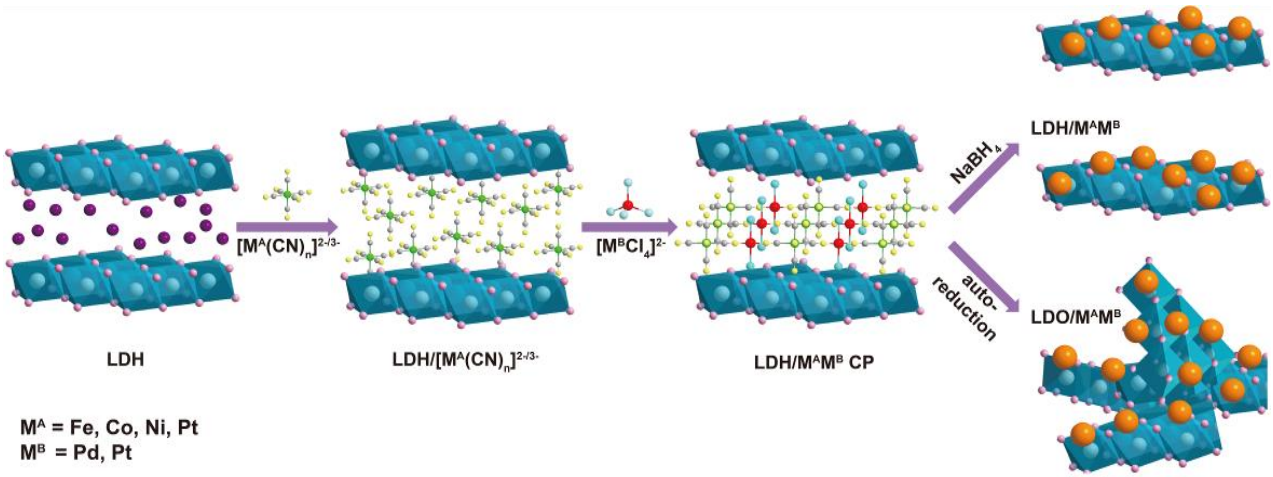

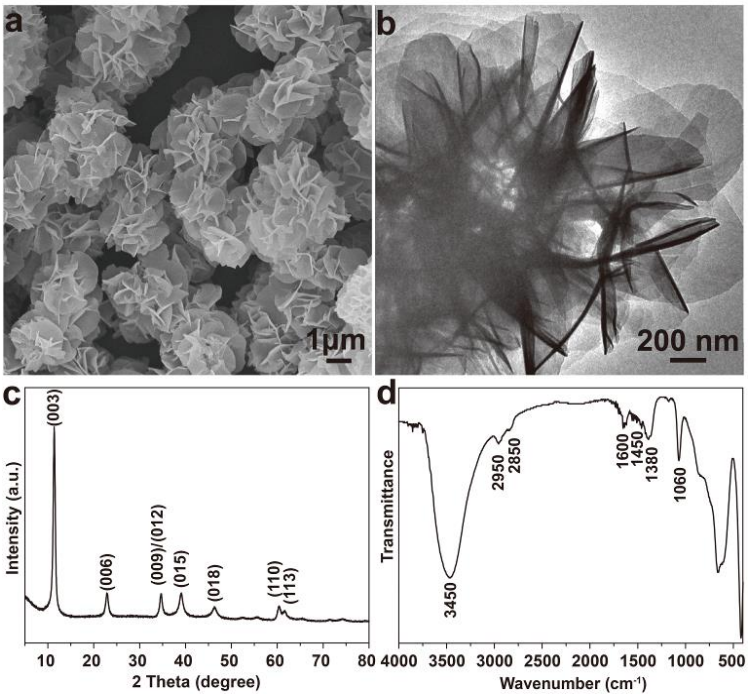

Figure 1. (a) SEM image, (b) TEM image, (c) XRD pattern and (d) FTIR spectrum of flowerlike MgAl-LDH spheres.

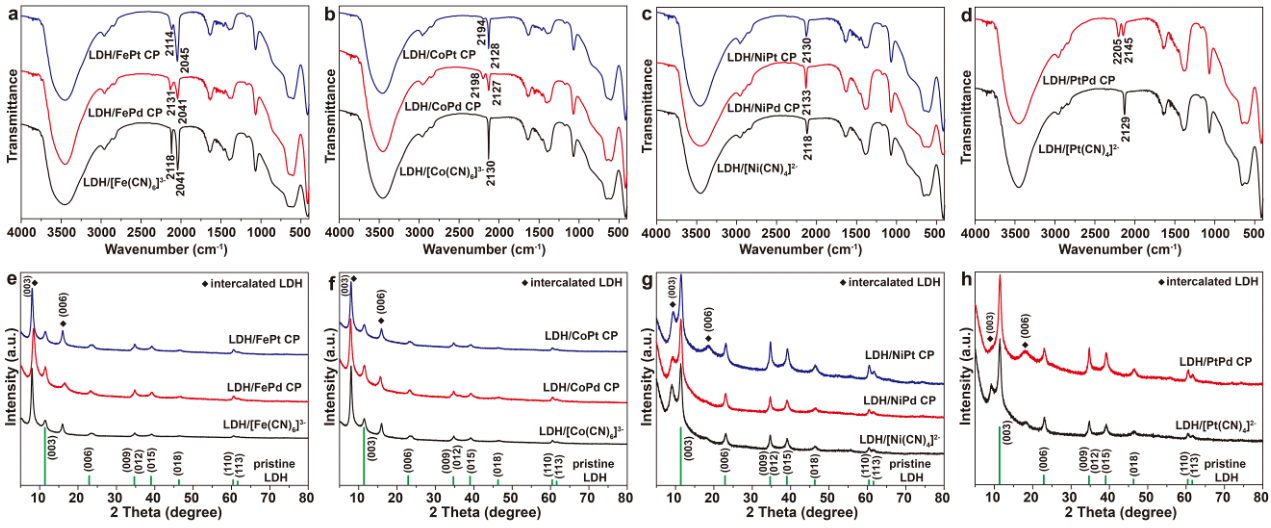

Figure 2. (a-d) FTIR spectra and (e-h) XRD patterns of LDH/$[M^{A}(CN)_{n}]^{2-/3-}$ and LDH/$M^{A}M^{B}$ CP (♦: (003) and (006) peaks of the intercalated LDH species).

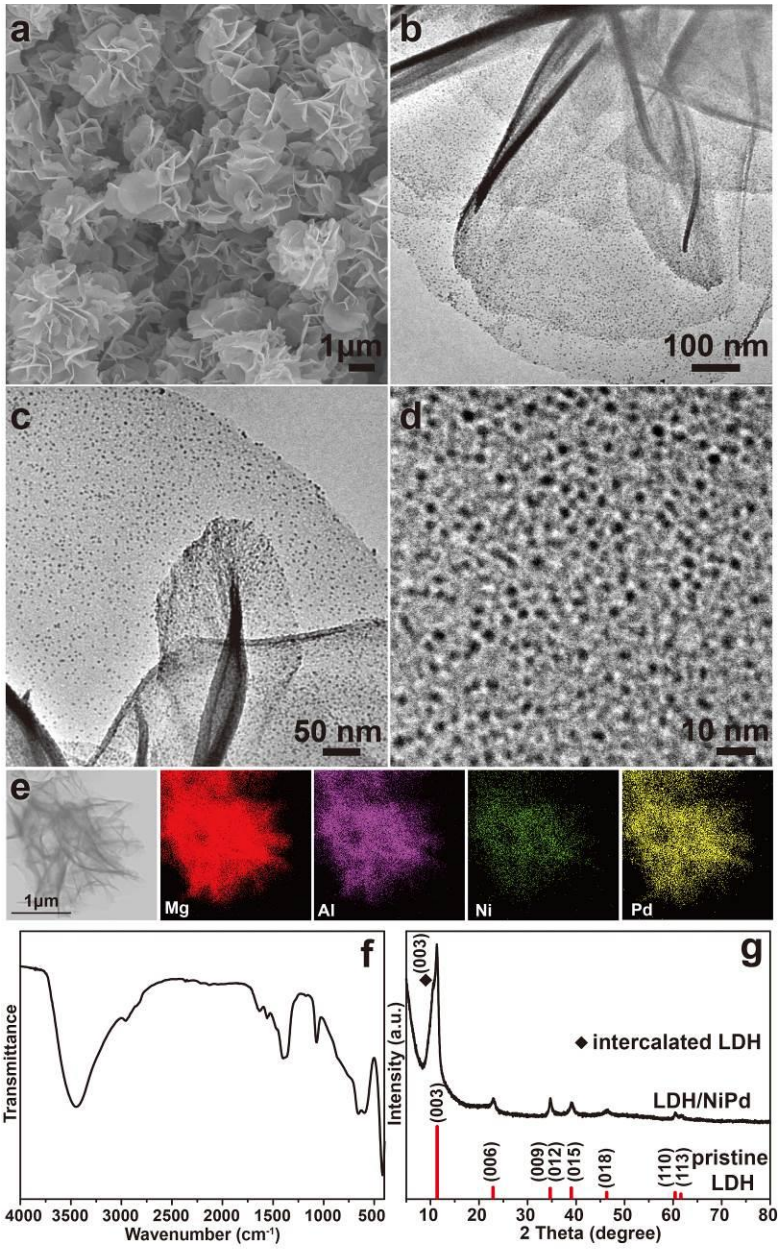

Figure 3. (a) SEM image, (b-d) TEM images, (e) EDX elemental mapping, (f) FTIR spectrum, and (g) XRD pattern of LDH/NiPd composite (♦: (003) peak of the intercalated LDH species).

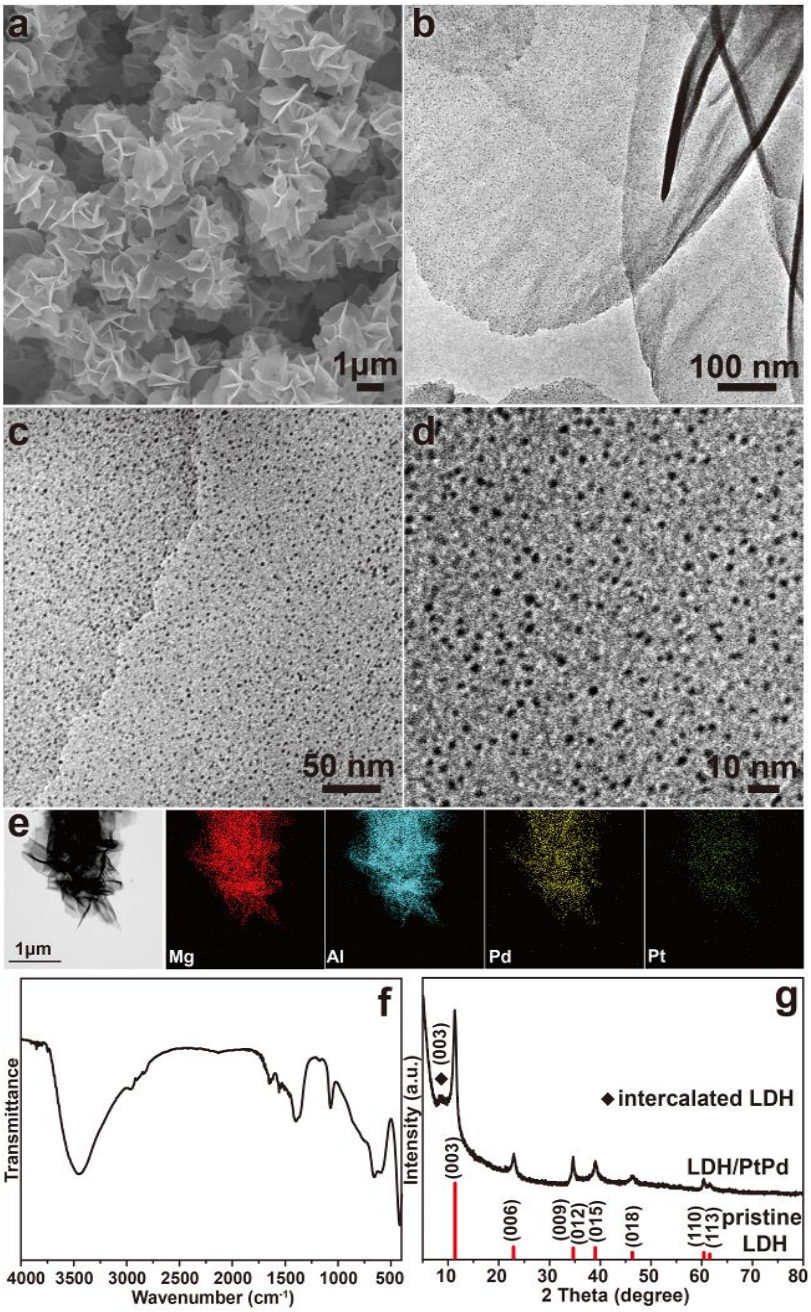

Figure 4. (a) SEM image, (b-d) TEM images, (e) EDX elemental mapping, (f) FTIR spectrum and (g) XRD pattern of LDH/PtPd composite (♦: (003) peak of the intercalated LDH species). Similar characterization results were observed for LDH/FePd, LDH/FePt, LDH/CoPd, LDH/CoPt and LDH/NiP t (*i.e.*, LDH/M^AM^B type); see Figures S8-S12 for details.

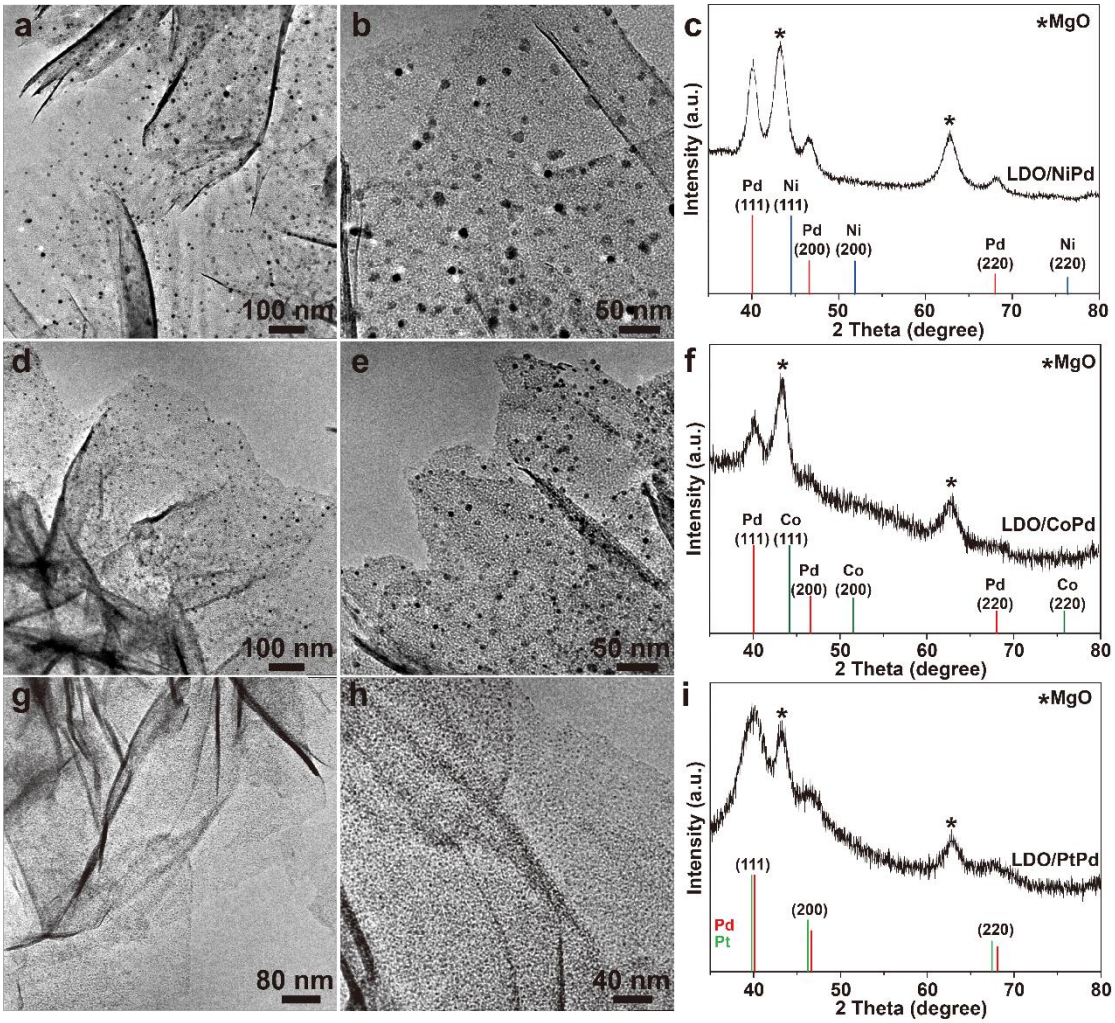

Figure 5. TEM images and XRD patterns of (a-c) LDO/NiPd, (d-f) LDO/CoPd and (g-i) LDO/PtPd. For XRD patterns, no peaks were present below $2\theta = 35°$.

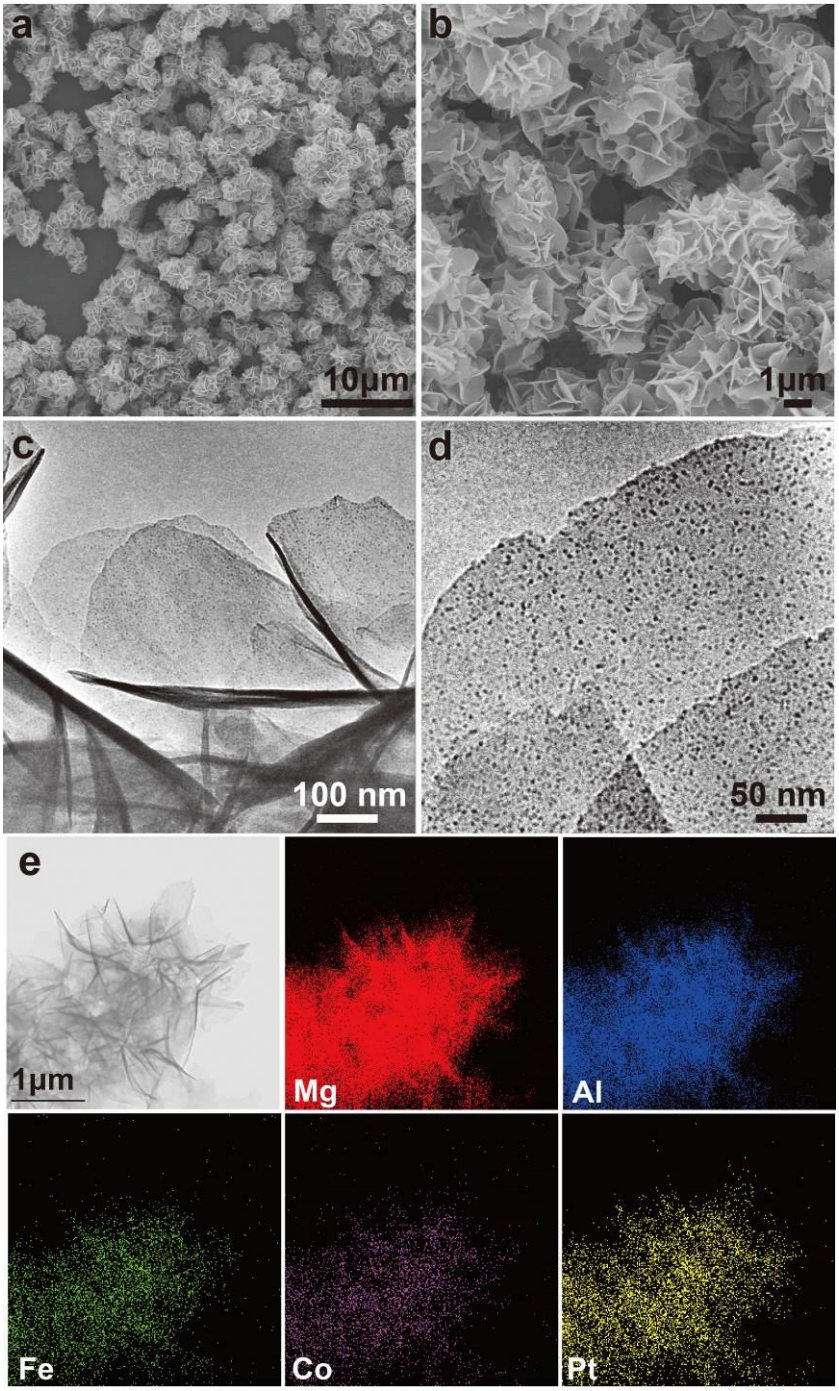

Figure 6. (a) SEM image, (b-d) TEM images and (e) EDX elemental mapping of LDH/FeCoPt composite. Similar characterization results were observed for LDH/FePdPt, LDH/FeNiPt and LDH/NiCoPt (*i.e.*, LDH/$M^AM^BM^C$ type), see Figures S15-S17 for details.

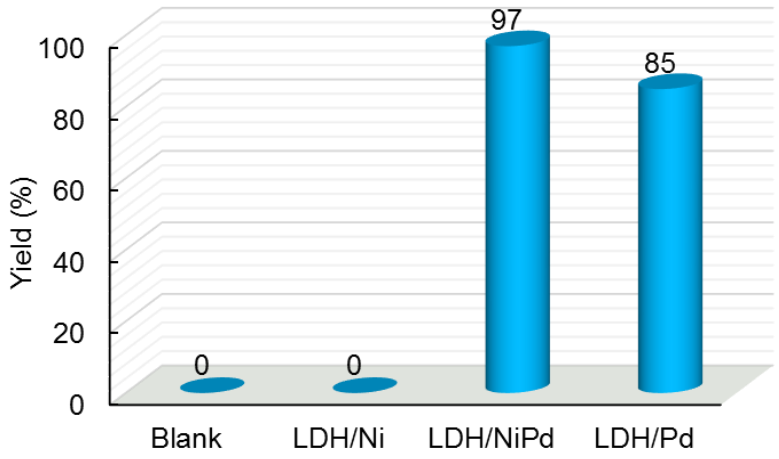

Figure 7. Yield of the coupling reaction between iodobenzene and phenylboronic acid in the presence of different catalysts: blank, LDH/Ni, LDH/NiPd and LDH/Pd. Reaction conditions: iodobenzene (0.5 mmol), phenylboronic acid (1.0 mmol), K_2CO_3 (2 mmol), ethanol (10 mL), catalyst (0.42 mol% Pd), reaction temperature: 80°C under atmospheric condition, reaction time: 30 min. For LDH/Ni case, 0.21 mol% Ni was used in the reaction.

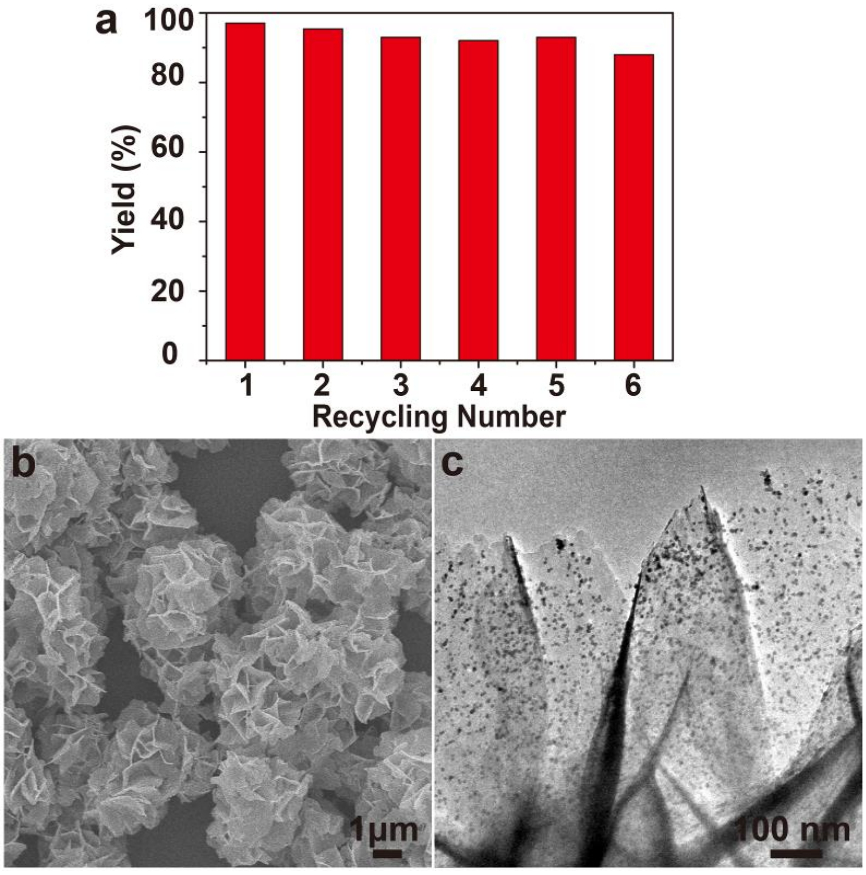

Figure 8. (a) Recycling test of the LDH/NiPd in the reaction between iodobenzene and phenylboronic acid. Reaction conditions: iodobenzene (0.5 mmol), phenylboronic acid (1.0 mmol), K_2CO_3 (2 mmol), ethanol (10 mL), LDH/NiPd (0.42 mol% Pd in the reaction system, atomic ratio of Ni/Pd = 1/2), reaction temperature: 80 °C under atmospheric condition, reaction time: 30 min. (b) SEM image and (c) TEM image of LDH/NiPd after being used repetitively for 6 times.

Table 1. Suzuki–Miyaura cross-coupling reactions catalyzed by LDH/NiPd nanocomposite.[a)]

Entry	ArX	Time (min)	Yield (%)
1		30	97.0
2	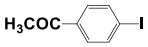	15	~100
3	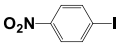	15	~100
4	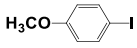	30	96.6
5	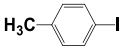	30	96.5
6		60	70.6
7	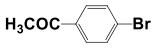	60	92.3

[a)] Reaction conditions: ArX (0.5 mmol), Ph-B(OH)$_2$ (1.0 mmol), K_2CO_3 (2 mmol), ethanol (10 mL), LDH/NiPd (0.42 mol% Pd in the reaction system; atomic ratio of Ni/Pd = 1/2), 80 °C under atmospheric condition.

A novel and versatile approach to construct supported ultrafine alloy nanoparticles from two-dimensional intercalated coordination polymers in layered double hydroxide (LDH) is developed via simultaneous intercalation and coordination process followed with subsequent reduction. To demonstrate their workability, one class of the resulting supported alloy nanoparticles (LDH/NiPd nanocomposite), is explored to catalyze cross coupling reactions.

layered double hydroxide, intercalation chemistry, coordination polymer, alloy nanoparticle, cross coupling reaction

Ping Li, Wen Liu, John S. Dennis, and Hua Chun Zeng*

Ultrafine Alloy Nanoparticles Converted from Two-Dimensional Intercalated Coordination Polymers for Catalytic Application

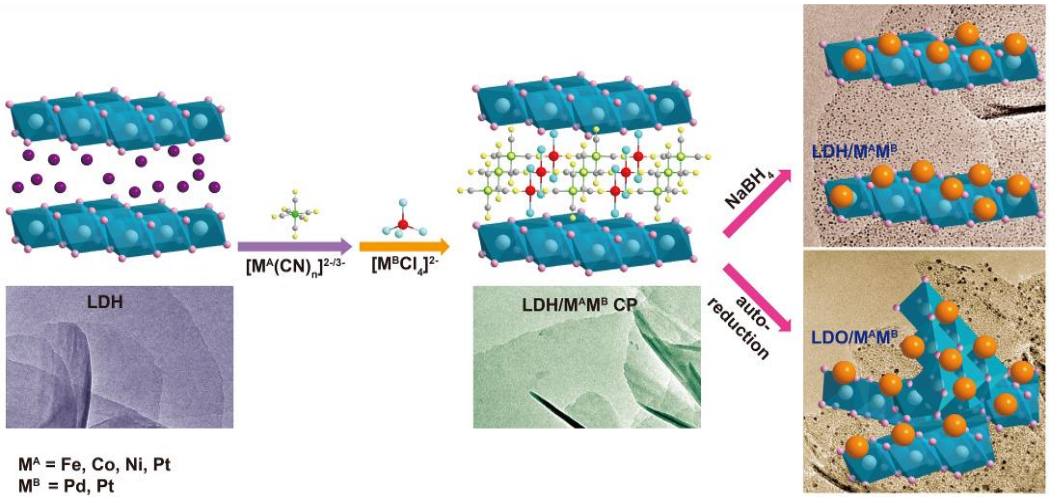

Supporting Information

Ultrafine Alloy Nanoparticles Converted from Two-Dimensional Intercalated Coordination Polymers for Catalytic Application

*Ping Li, Wen Liu, John S. Dennis, and Hua Chun Zeng**

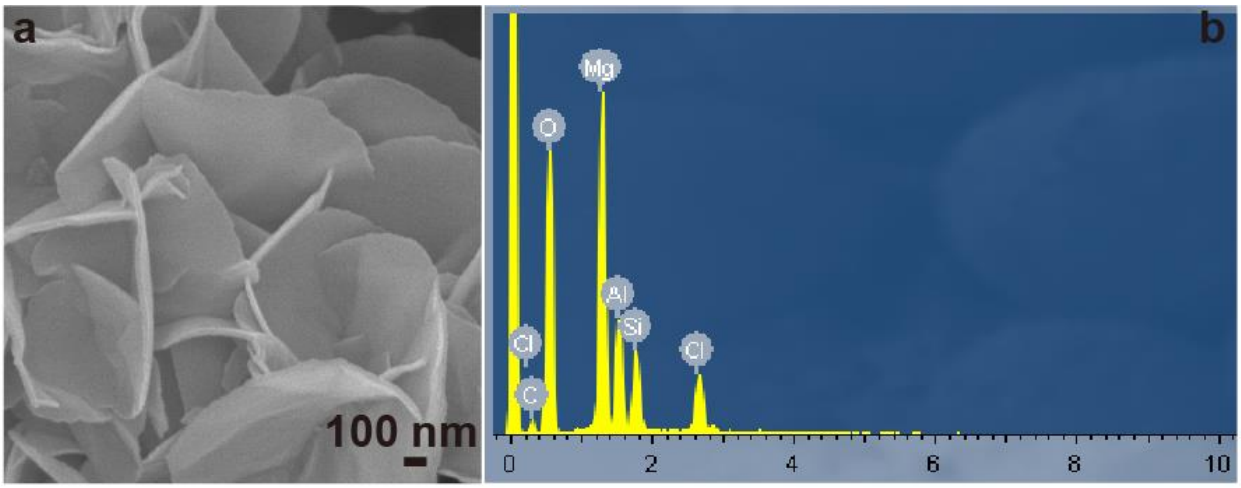

Figure S1. (a) SEM image and (b) EDX spectrum of MgAl-LDH flowerlike spheres. The Si element is from the silicon wafer.

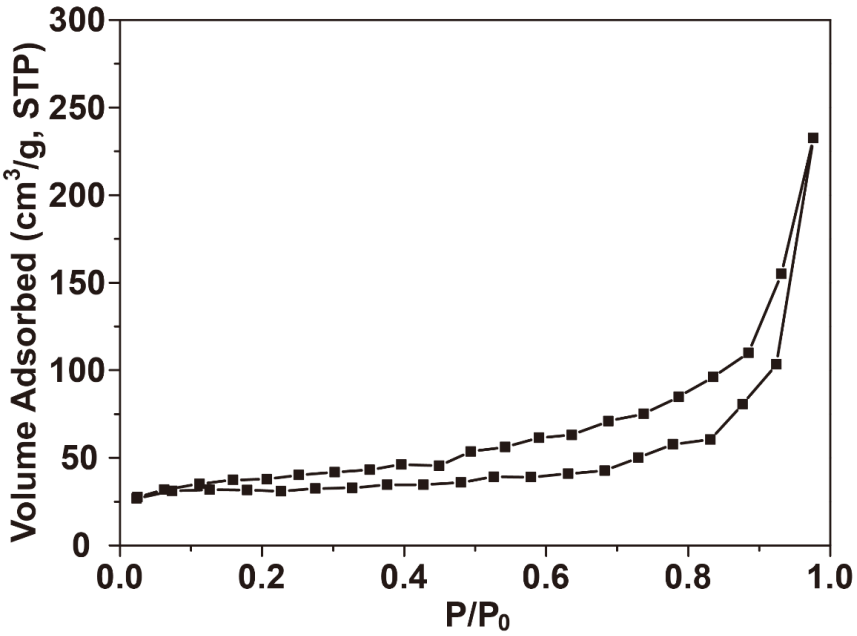

Figure S2. N_2 adsorption–desorption isotherm of MgAl–LDH sample.

Additional experimental details for the preparation of LDH/M^AM^B and LDH/$M^AM^BM^C$:

Table S1. The amount of metal precursors used in the preparation of LDH/M^AM^B nanocomposites

LDH/M^AM^B	**n (metal precursor)/mmol**	
	$[M^A(CN)_n]^{2-/3-}$	**$[M^BCl_4]^{2-}$**
LDH/FePd	0.05 mmol $K_3[Fe(CN)_6]$	0.05 mmol Na_2PdCl_4
LDH/FePt	0.05 mmol $K_3[Fe(CN)_6]$	0.05 mmol K_2PtCl_4
LDH/CoPd	0.05 mmol $K_3[Co(CN)_6]$	0.05 mmol Na_2PdCl_4
LDH/CoPt	0.05 mmol $K_3[Co(CN)_6]$	0.05 mmol K_2PtCl_4
LDH/NiPd	0.025 mmol $K_2[Ni(CN)_4]$	0.05 mmol Na_2PdCl_4
LDH/NiPt	0.025 mmol $K_2[Ni(CN)_4]$	0.05 mmol K_2PtCl_4
LDH/PtPd	0.025 mmol $K_2[Pt(CN)_4]$	0.025 mmol Na_2PdCl_4

Table S2. The amount of metal precursors used in the preparation of LDH/$M^AM^BM^C$ nanocomposites

LDH/$M^AM^BM^C$	**n (metal precursor)/mmol**		
LDH/FePdPt	0.05 mmol $K_3[Fe(CN)_6]$	0.025 mmol Na_2PdCl_4	0.025 mmol K_2PtCl_4
LDH/FeNiPt	0.025 mmol $K_3[Fe(CN)_6]$	0.025 mmol $K_2[Ni(CN)_4]$	0.05 mmol K_2PtCl_4
LDH/FeCoPt	0.025 mmol $K_3[Fe(CN)_6]$	0.025 mmol $K_3[Co(CN)_6]$	0.05 mmol K_2PtCl_4
LDH/NiCoPt	0.025 mmol $K_2[Ni(CN)_4]$	0.025 mmol $K_3[Co(CN)_6]$	0.05 mmol K_2PtCl_4

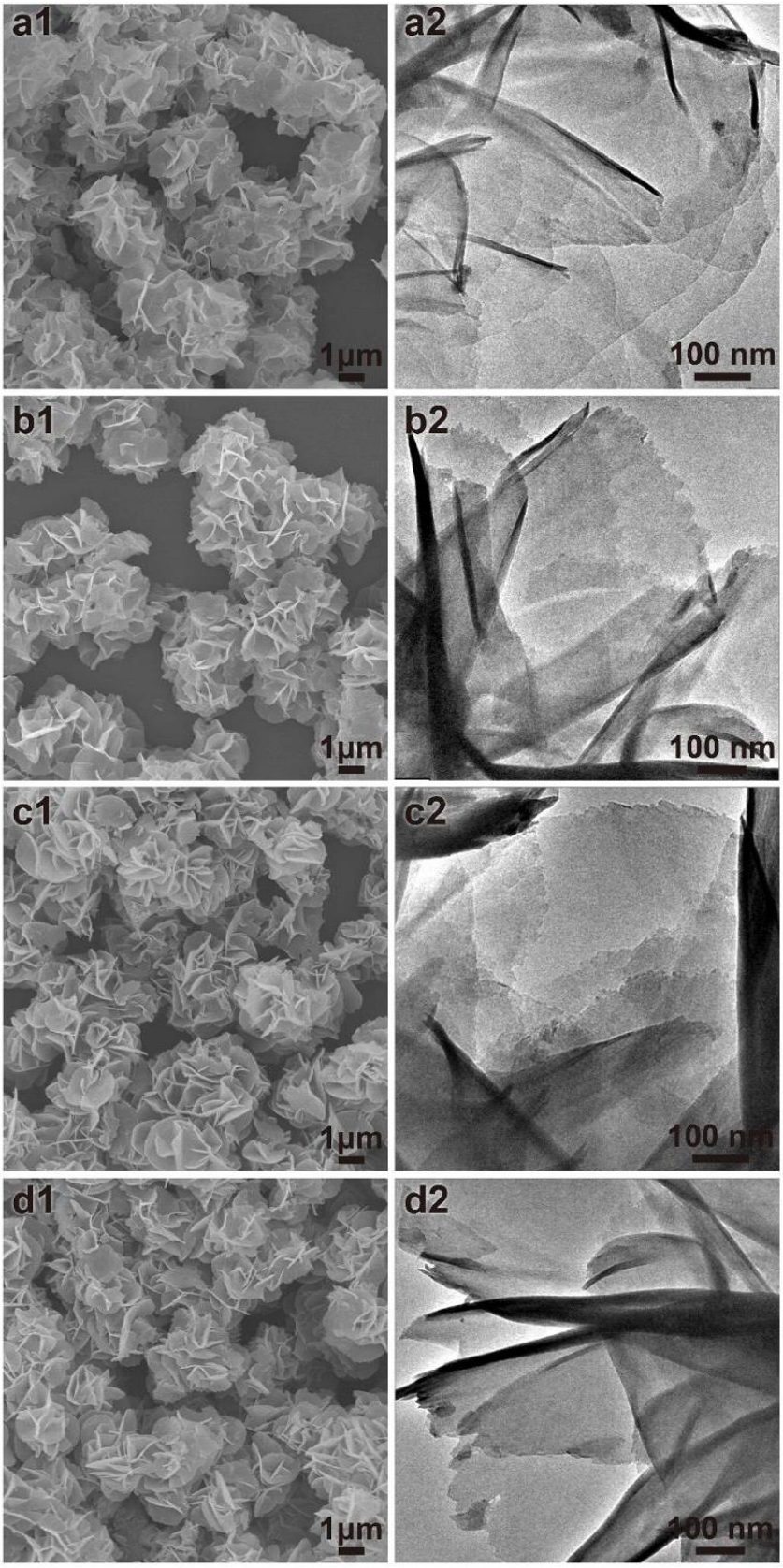

Figure S3. (1) SEM and (2) TEM images of LDH/M^AM^B CP: (a) LDH/FePd CP, (b) LDH/FePt CP, (c) LDH/CoPd CP, and (d) LDH/CoPt CP.

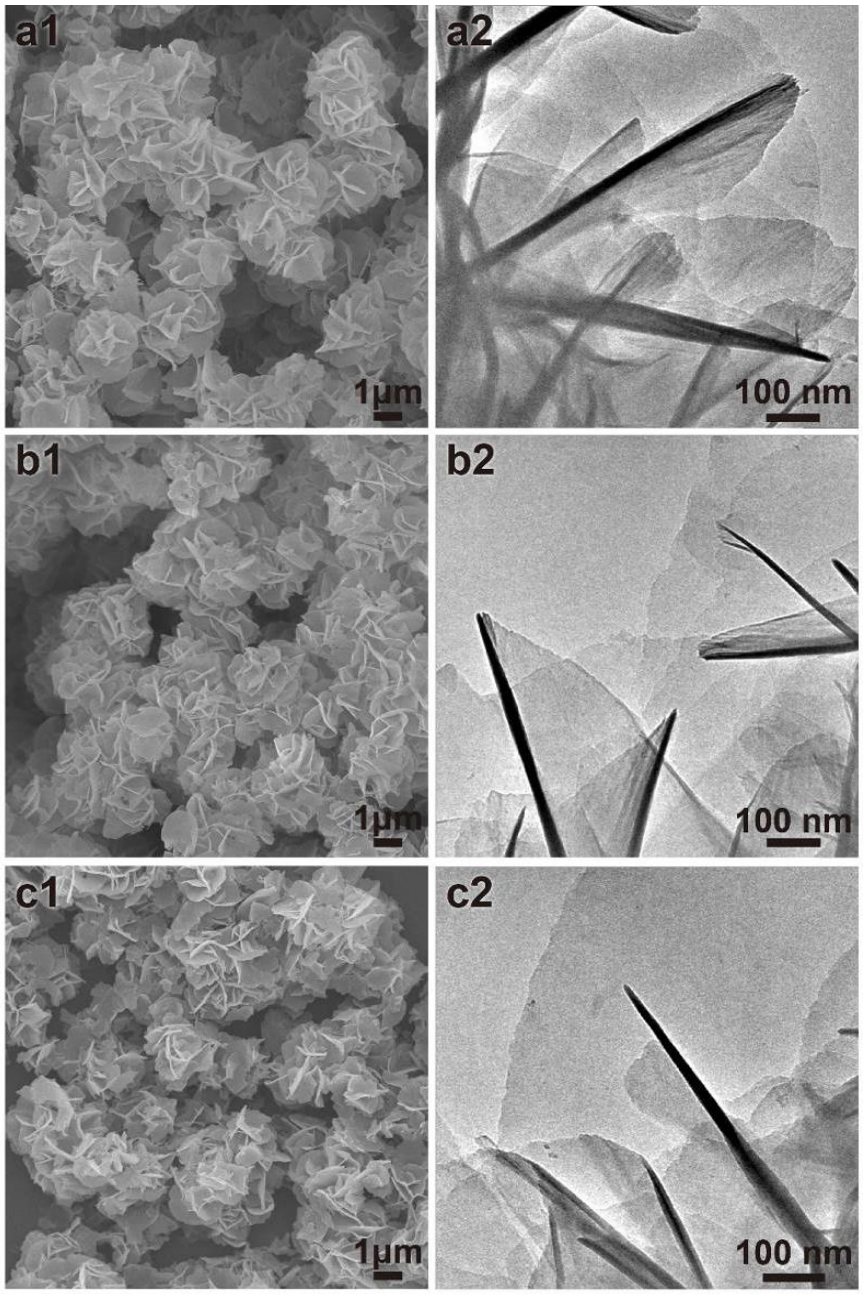

Figure S4. (1) SEM and (2) TEM images of LDH/M^AM^B CP: (a) LDH/NiPd CP, (b) LDH/NiPt CP, and (c) LDH/PtPd CP.

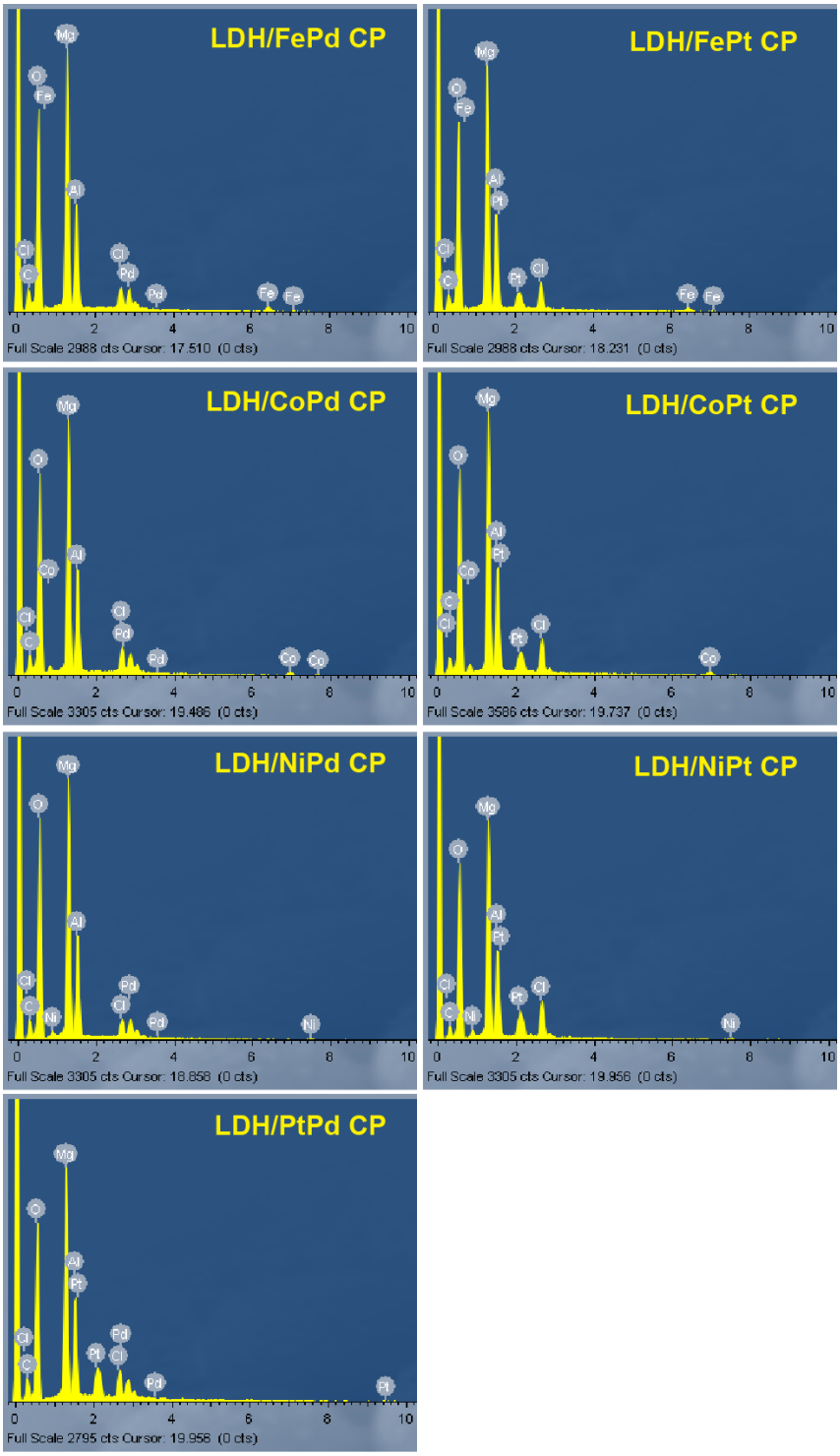

Figure S5. EDX spectra of LDH/M^AM^B CP (where M^AM^B = FePd, FePt, CoPd, CoPt, NiPd, NiPt and PtPd).

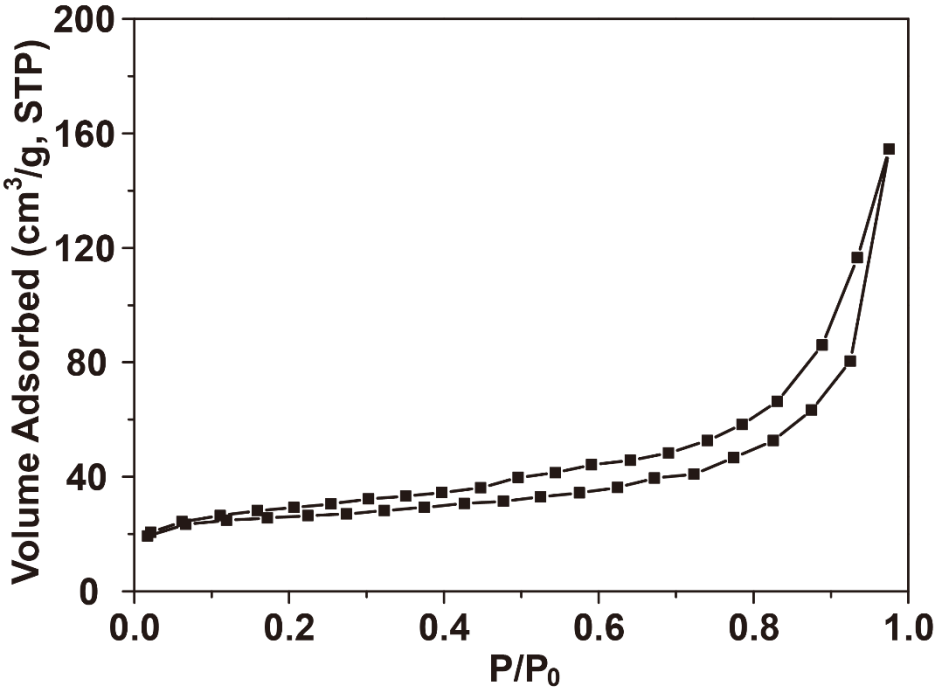

Figure S6. N_2 adsorption–desorption isotherm of LDH/NiPd nanocomposite.

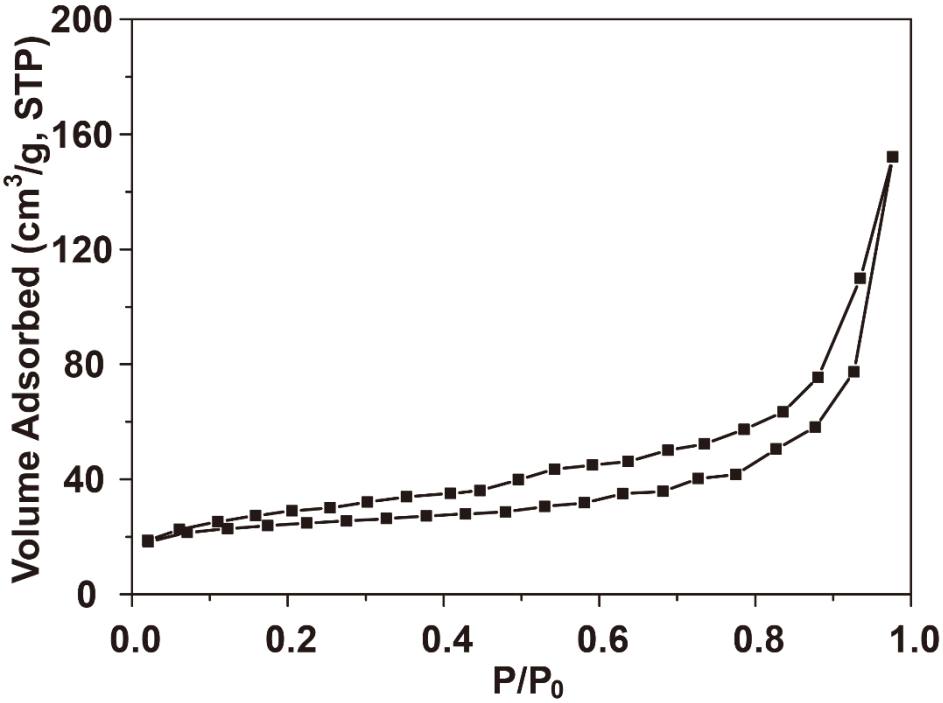

Figure S7. N_2 adsorption–desorption isotherm of LDH/PtPd nanocomposite.

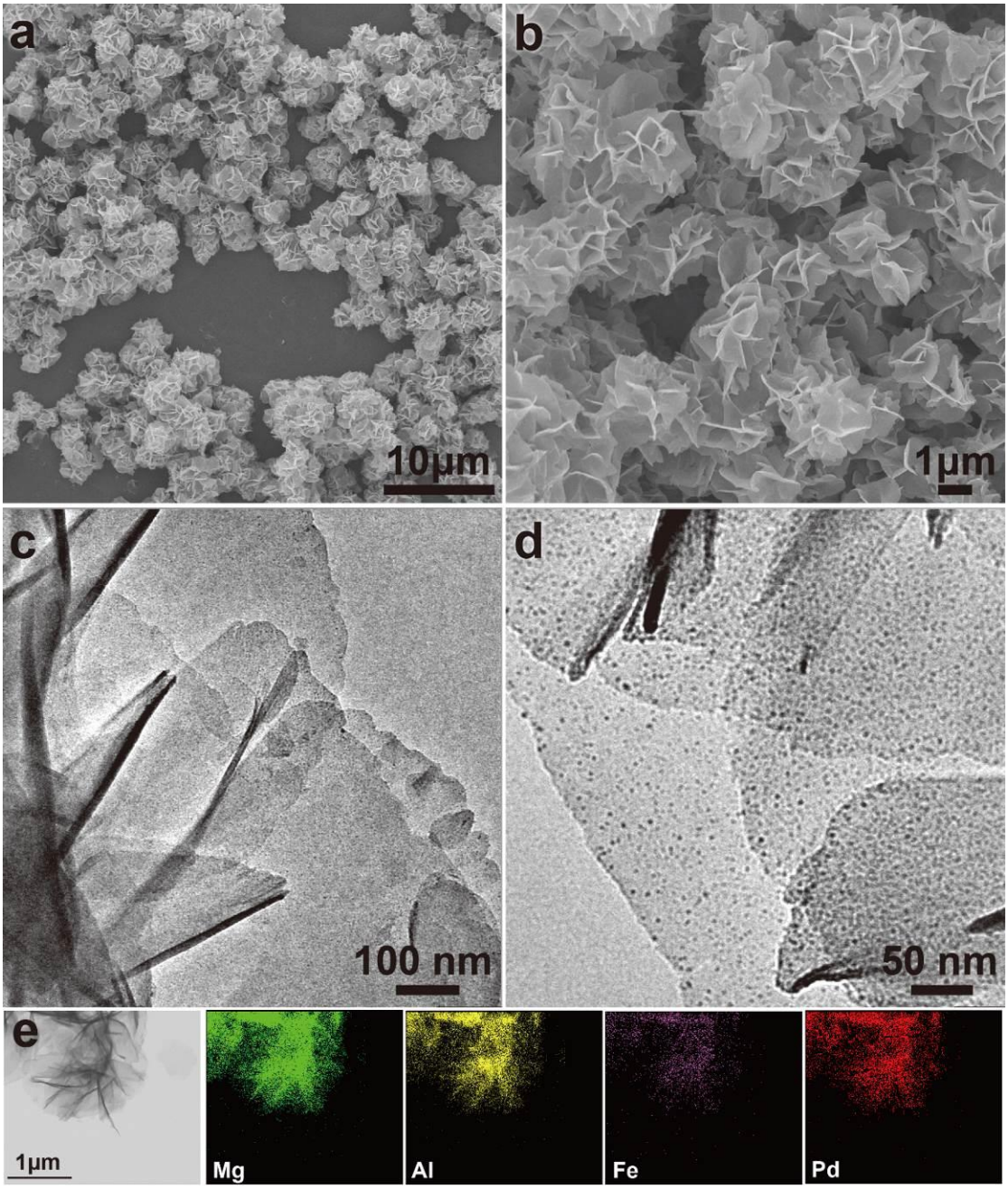

Figure S8. (a, b) SEM images, (c, d) TEM images, and (e) EDX elemental mapping of LDH/FePd nanocomposite.

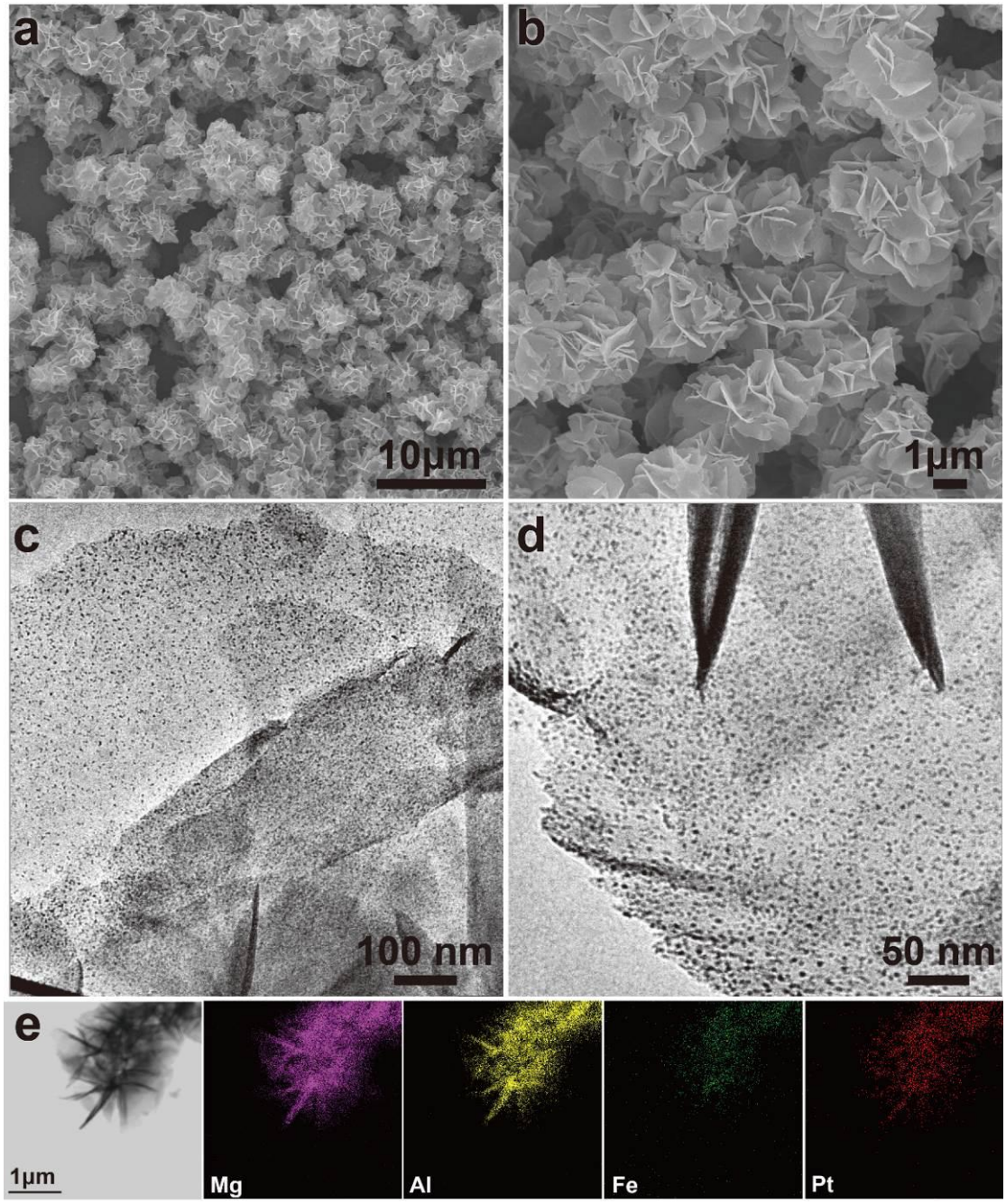

Figure S9. (a, b) SEM images, (c, d) TEM images, and (e) EDX elemental mapping of LDH/FePt nanocomposite.

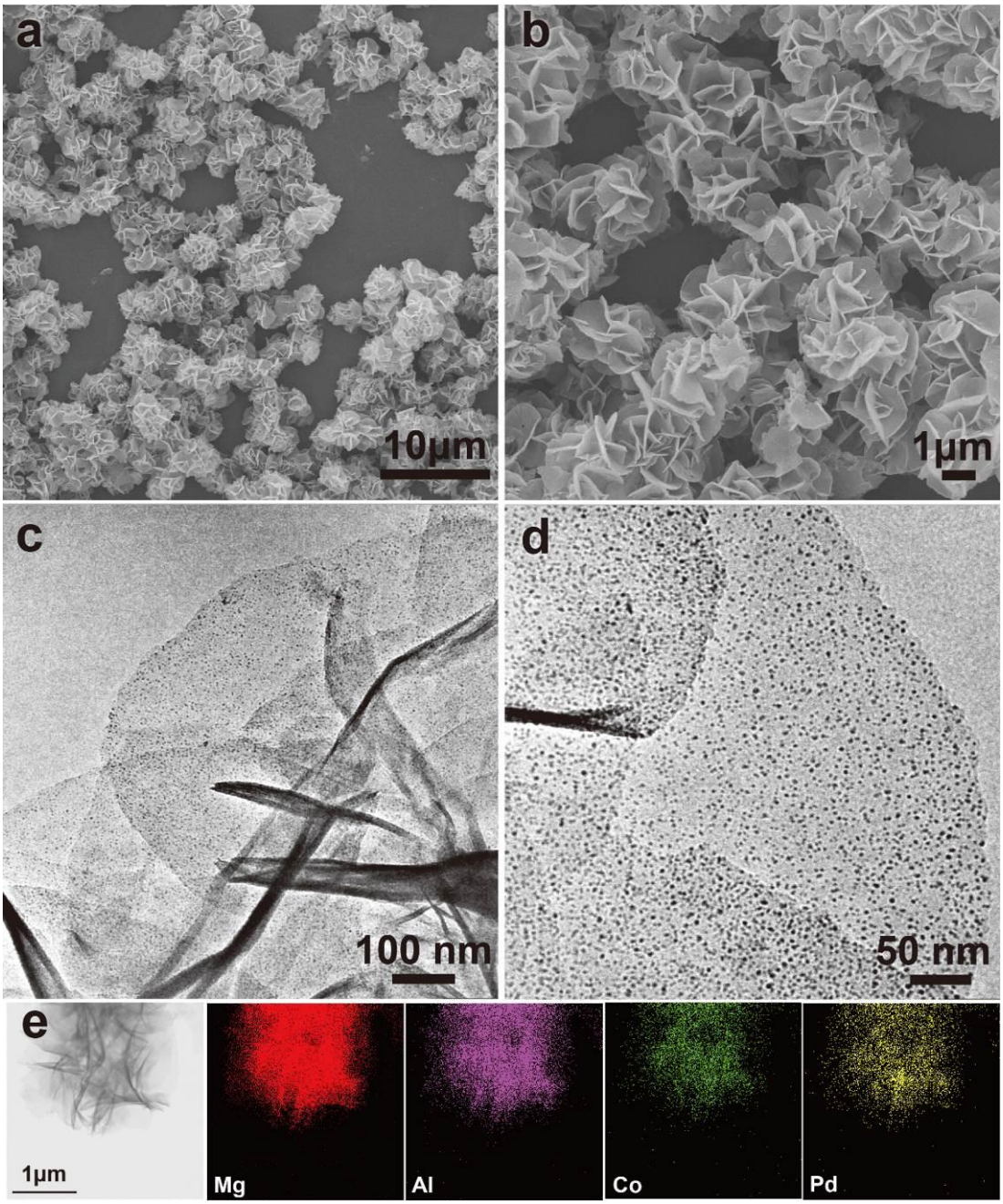

Figure S10. (a, b) SEM images, (c, d) TEM images, and (e) EDX elemental mapping of LDH/CoPd nanocomposite.

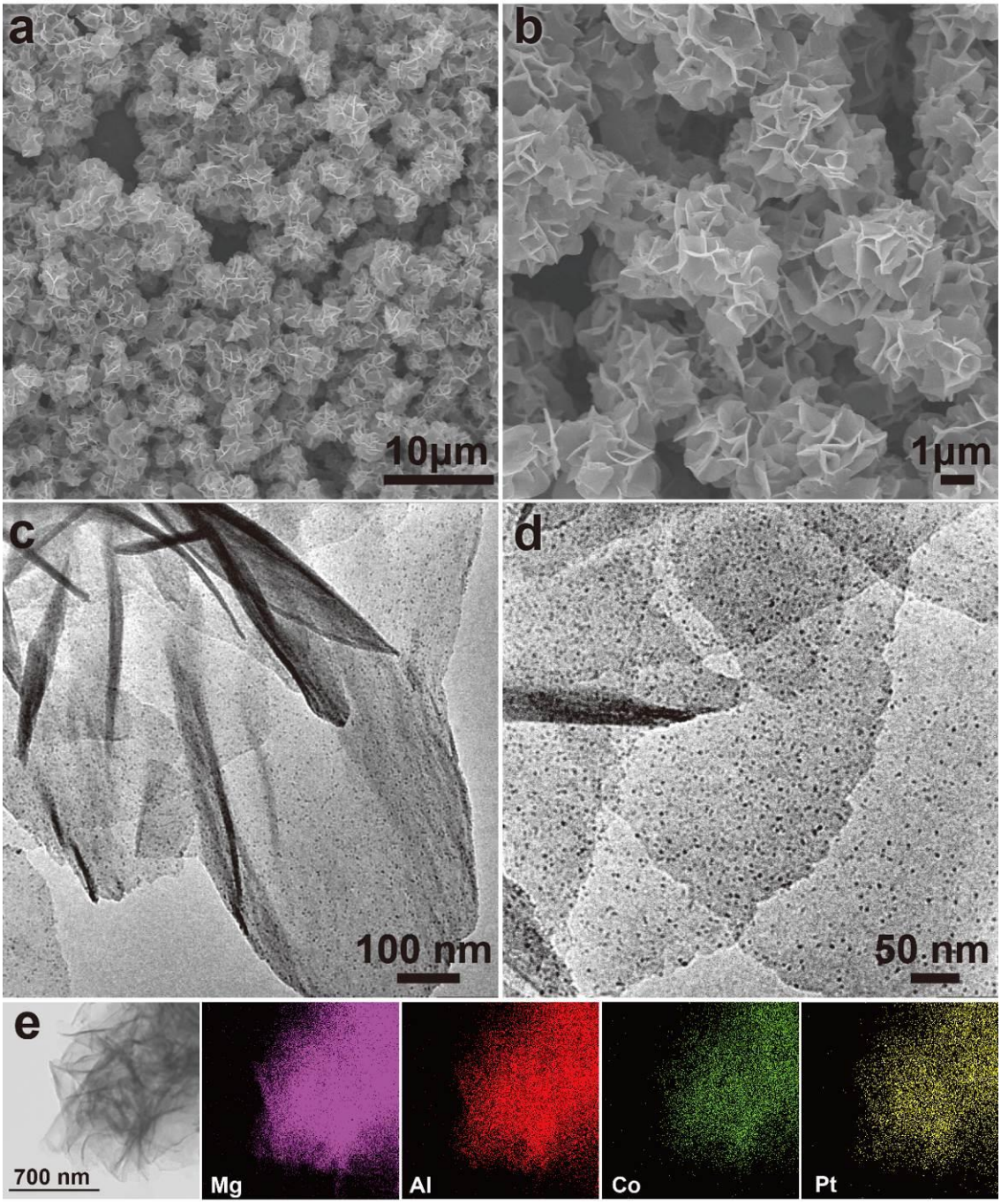

Figure S11. (a, b) SEM images, (c, d) TEM images, and (e) EDX elemental mapping of LDH/CoPt nanocomposite.

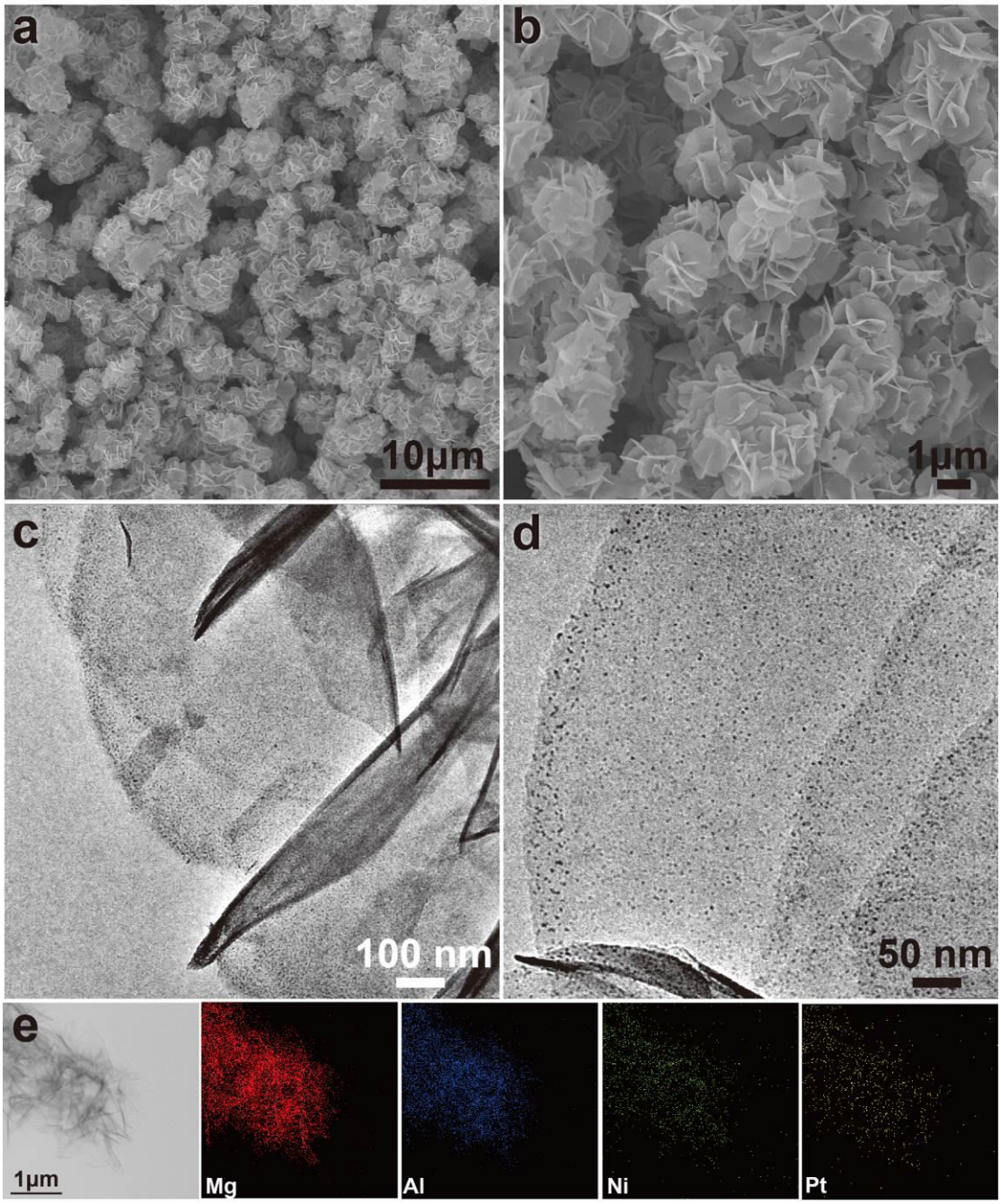

Figure S12. (a, b) SEM images, (c, d) TEM images, and (e) EDX elemental mapping of LDH/NiPt nanocomposite.

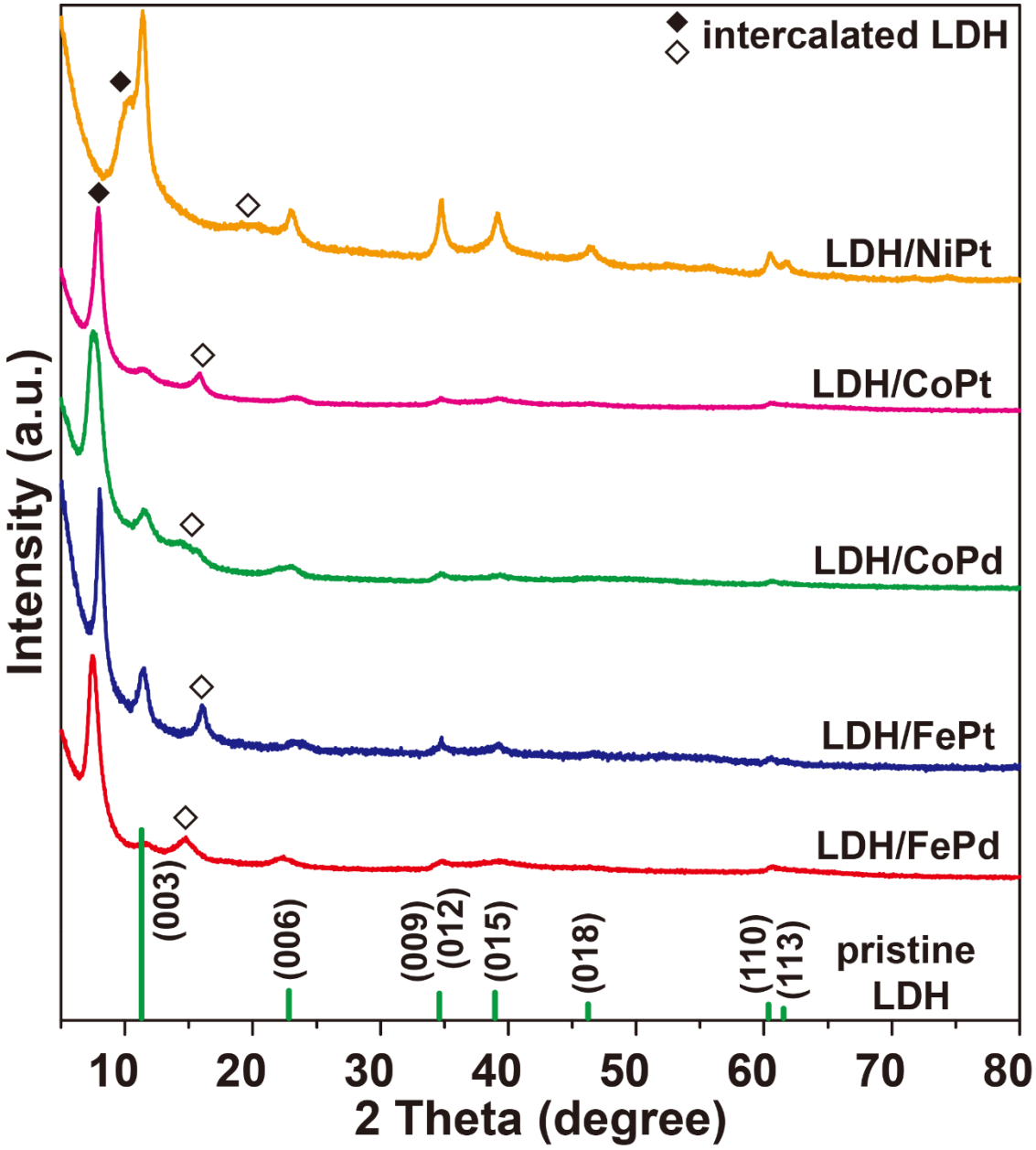

Figure S13. XRD patterns of LDH/FePd, LDH/FePt, LDH/CoPd, LDH/CoPt, and LDH/NiPt nanocomposites. (♦: (003) peak of the intercalated LDH species; ◊: (006) peak of the intercalated LDH species).

Table S3. The chemical compositions of LDH/M^AM^B samples obtained from ICP-AES analysis.

LDH/M^AM^B	$[M^A(CN)_n]^{2-/3-}$	$[M^BCl_4]^{2-}$	Mg (wt%)	Al (wt%)	M^A (wt%)	M^B (wt%)
LDH/FePd	$K_3[Fe(CN)_6]$	Na_2PdCl_4	15.58	8.16	2.14	3.7
LDH/FePt	$K_3[Fe(CN)_6]$	K_2PtCl_4	16.46	8.74	2.01	3.6
LDH/CoPd	$K_3[Co(CN)_6]$	Na_2PdCl_4	16.23	8.34	1.63	2.41
LDH/CoPt	$K_3[Co(CN)_6]$	K_2PtCl_4	16.94	8.41	1.74	5.39
LDH/NiPd	$K_2[Ni(CN)_4]$	Na_2PdCl_4	16.44	8.67	1.14	3.82
LDH/NiPt	$K_2[Ni(CN)_4]$	K_2PtCl_4	16.43	8.74	1.00	6.03
LDH/PtPd	$K_2[Pt(CN)_4]$	Na_2PdCl_4	16.11	8.47	3.09	2.05

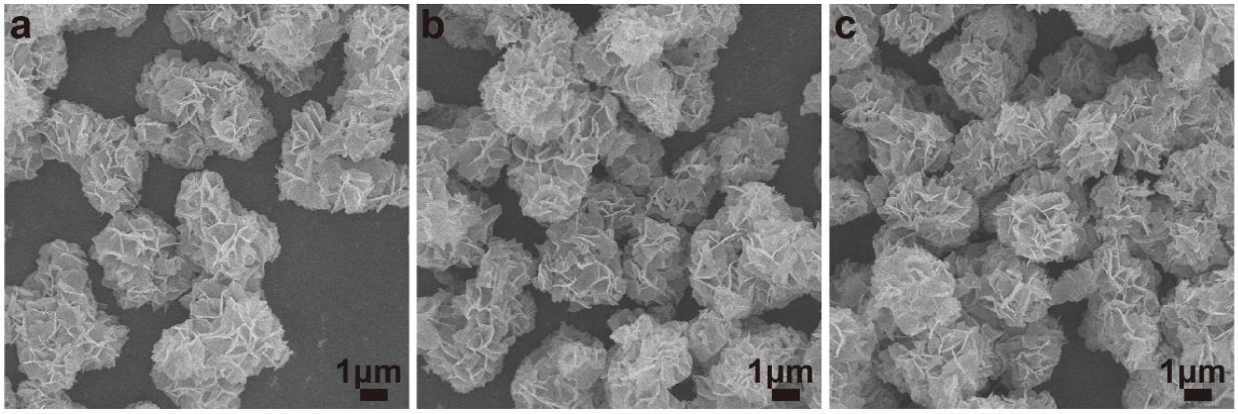

Figure S14. SEM images of (a) LDO/NiPd, (b) LDO/CoPd, and (c) LDO/PtPd nanocomposites.

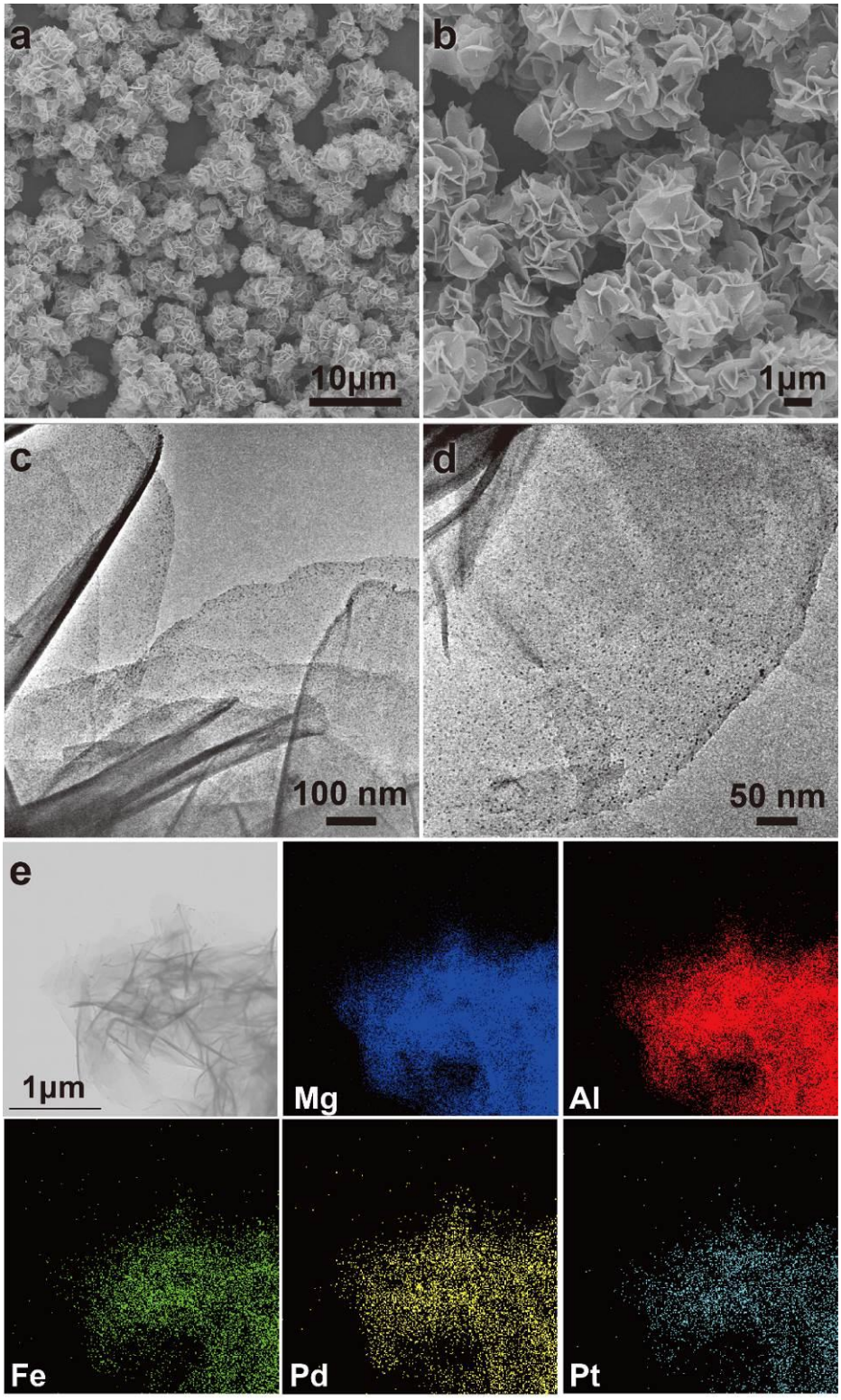

Figure S15. (a, b) SEM images, (c, d) TEM images, and (e) EDX elemental mapping of LDH/FePdPt nanocomposite.

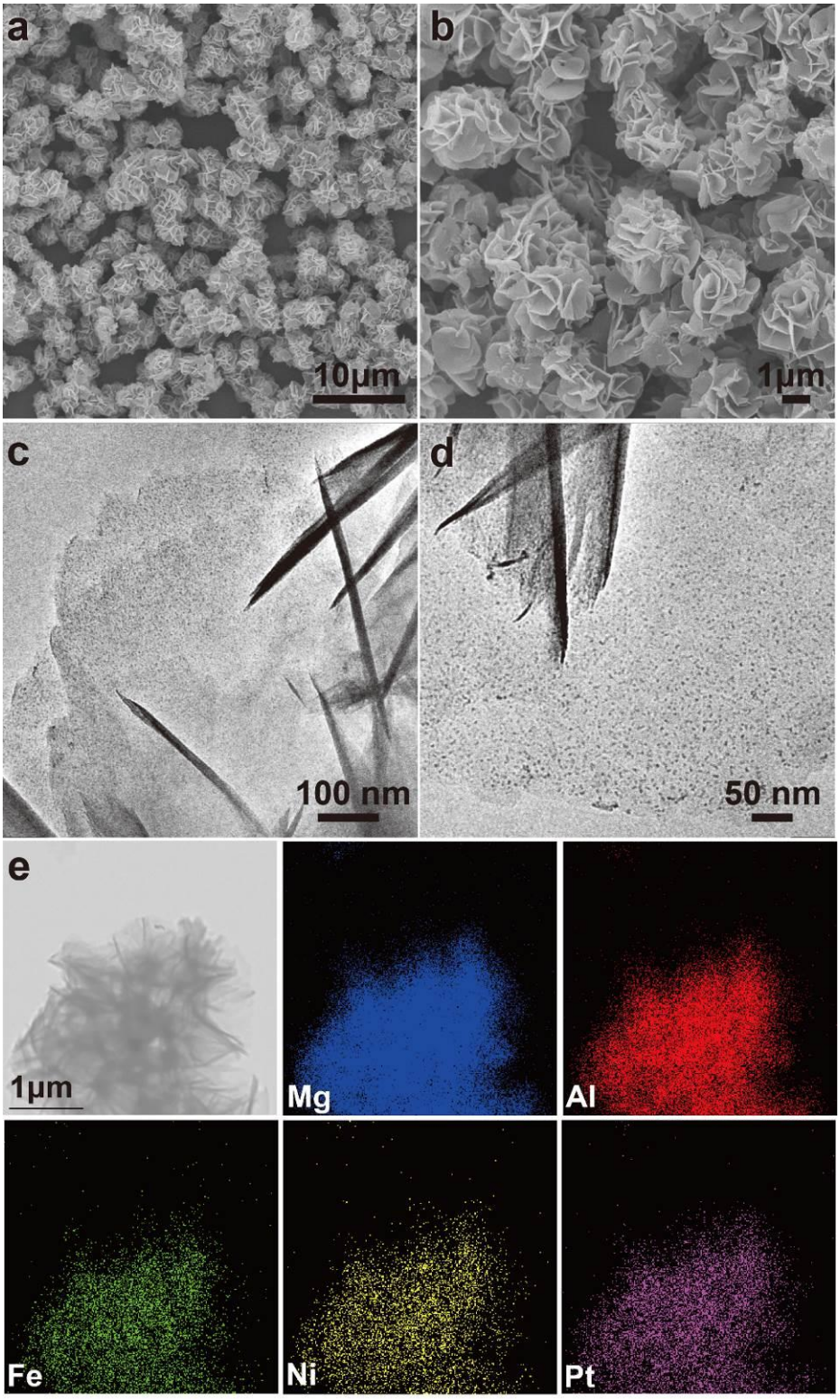

Figure S16. (a, b) SEM images, (c, d) TEM images, and (e) EDX elemental mapping of LDH/FeNiPt nanocomposite.

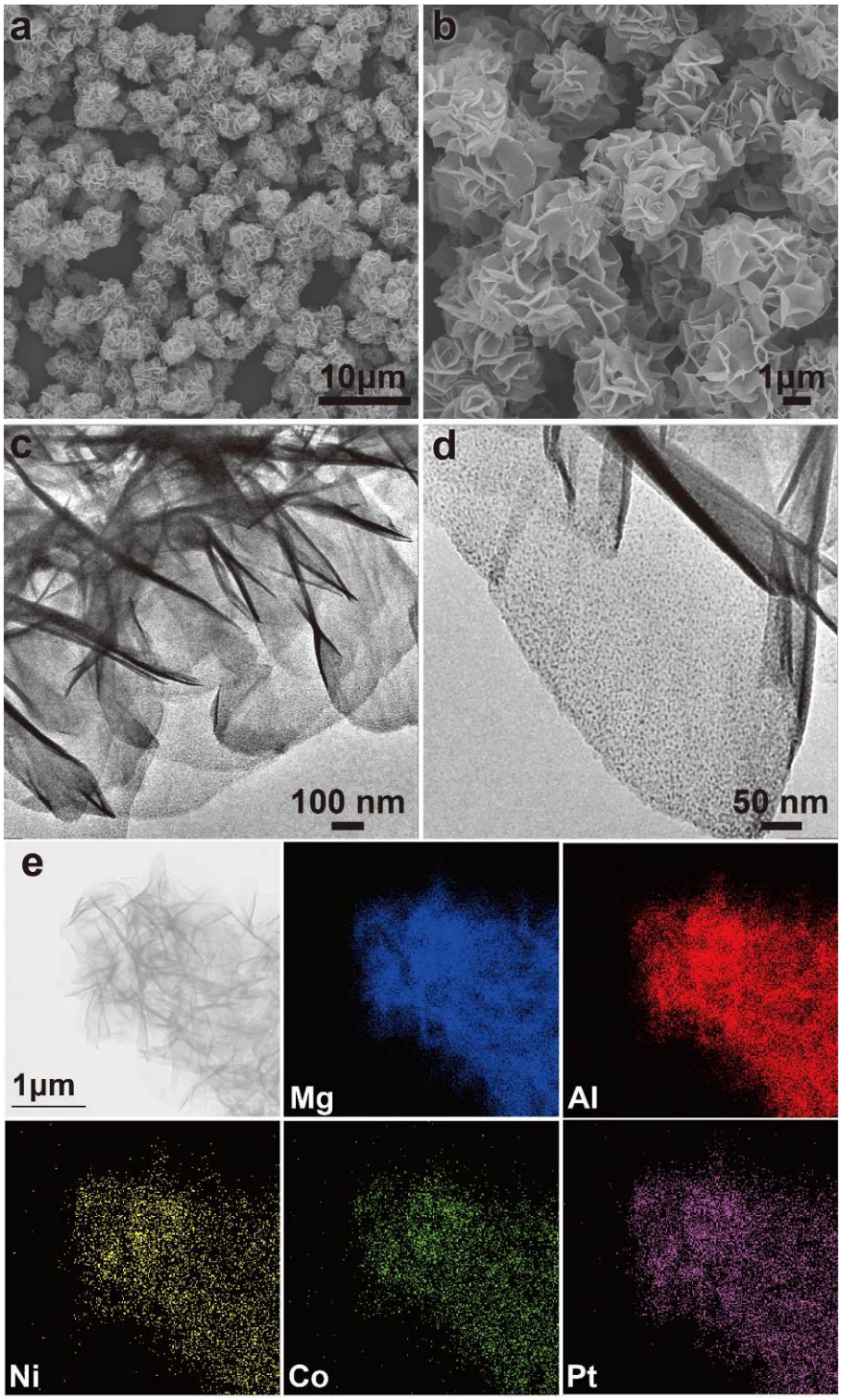

Figure S17. (a, b) SEM images, (c, d) TEM images, and (e) EDX elemental mapping of LDH/NiCoPt nanocomposite.

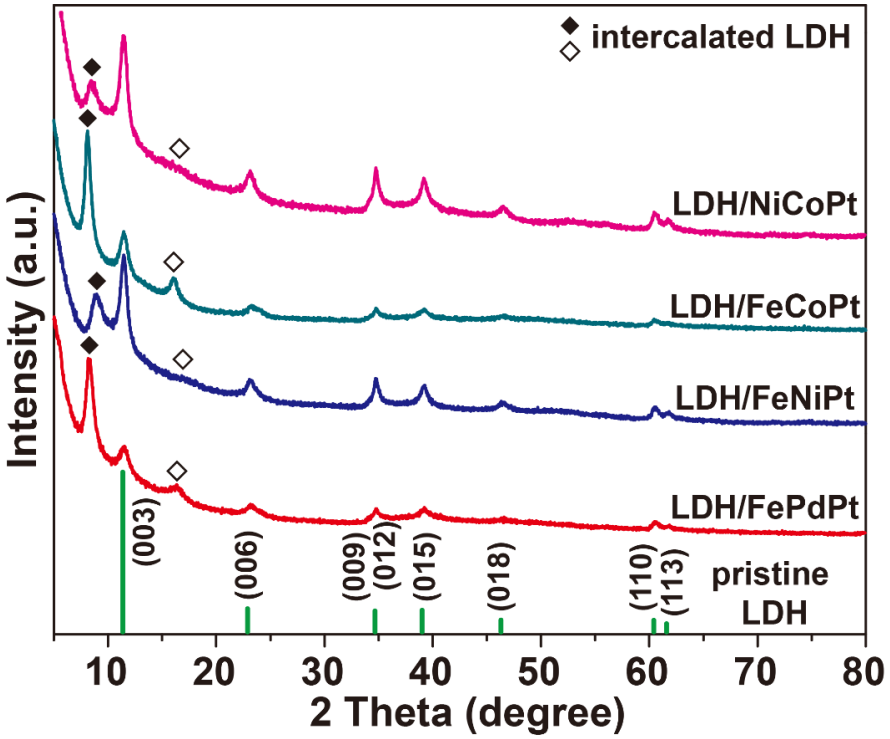

Figure S18. XRD patterns of LDH/FePdPt, LDH/FeNiPt, LDH/FeCoPt, and LDH/NiCoPt nanocomposites. (♦: (003) peak of the intercalated LDH species; ◊: (006) peak of the intercalated LDH species).

Table S4. The chemical compositions of LDH/$M^AM^BM^C$ samples obtained from ICP-AES analysis.

LDH/$M^AM^BM^C$	**metal precursors**	**Mg (wt%)**	**Al (wt%)**	**M^A (wt%)**	**M^B (wt%)**	**M^c (wt%)**
LDH/FePdPt	$K_3[Fe(CN)_6]$ Na_2PdCl_4 K_2PtCl_4	14.74	7.70	2.1	1.72	2.69
LDH/FeNiPt	$K_3[Fe(CN)_6]$ $K_2[Ni(CN)_4]$ K_2PtCl_4	15.95	8.18	1.06	0.95	6.07
LDH/FeCoPt	$K_3[Fe(CN)_6]$ $K_3[Co(CN)_6]$ K_2PtCl_4	15.50	8.12	1.09	0.85	4.68
LDH/NiCoPt	$K_2[Ni(CN)_4]$ $K_3[Co(CN)_6]$ K_2PtCl_4	15.72	8.00	0.93	1.05	5.13

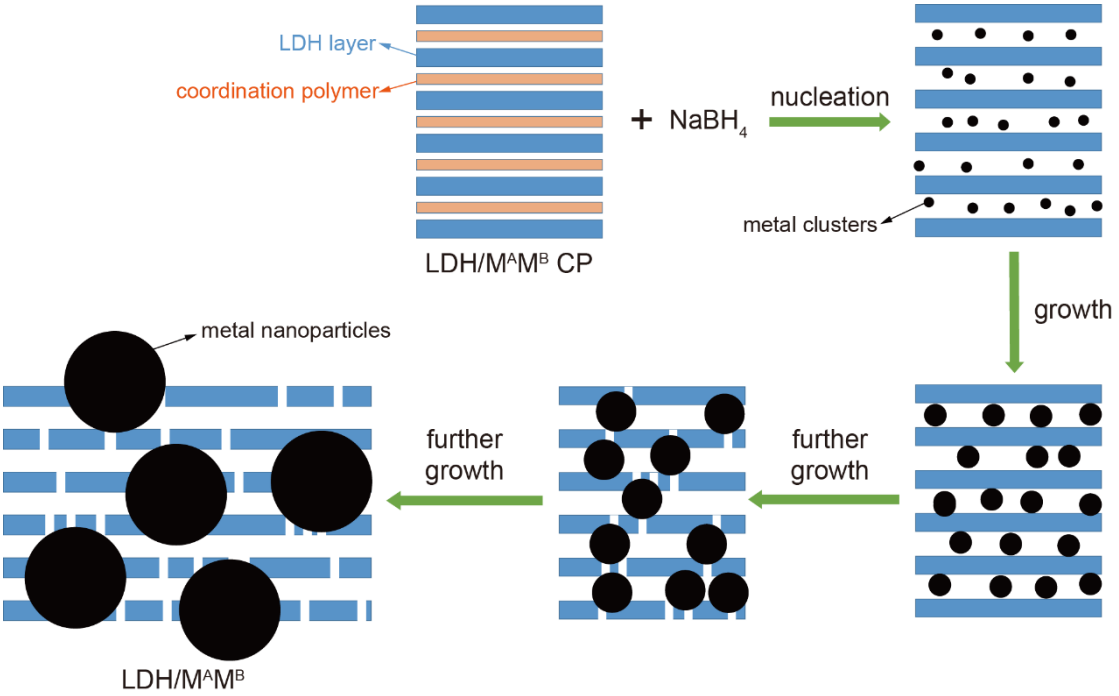

Scheme S1. The proposed formation process of LDH/M^AM^B nanocomposites (side views). In this illustration, the 2D-coordination polymer intercalated between LDH layers (i.e., brucite-like sheets) undergoes initial nucleation and various growth stages upon addition of reductant ($NaBH_4$). According to our TEM results, the metal clusters (i.e., metal nuclei) can further grow to 2-3 nm in size, embedding within or in the surface region of LDH structure, giving rise to final LDH/M^AM^B. In this process, the stress in the LDH layers develops gradually because of enlargement of metal nanoparticles in the gallery space, which also causes structural defects, noting that the metal nanoparticles can be formed across a few LDH layers. Such defects (or channels perpendicular to the layers) are apparently beneficial to chemical reactions, as metal nanoparticles can be easily accessed by the reactants.

Table S5. Comparison with other reported catalysts for Suzuki-Miyaura reaction between iodobenzene and phenylboronic acid.

Entry	Catalyst	Solvent	Base	Temp. (°C)	Time (h)	Yield (%)	TOF (h^{-1})	Ref.
1	**LDH/NiPd**	**EtOH**	**K_2CO_3**	**80**	**0.5**	**97**	**462**	**This work**
2	Pd/G-CNFs-900	EtOH	K_2CO_3	80	0.5	99.5	278.7	[1]
3	Hydroxyapatite/[Pd(COD)Cl_2]	H_2O	K_2CO_3	80	24	100	122.54	[2]
4	SBA-15/Met/Pd(II)	EtOH /H_2O	K_2CO_3	80	1	99	99	[3]
5	Porous Pd NPs	EtOH /H_2O	K_2CO_3	60	3	99.1	53.25	[4]
6	Pd-Fe_3O_4@C	EtOH	K_2CO_3	60	2	99	46.2	[5]
7	Pd/LDH	EtOH /H_2O	K_2CO_3	75	4	90	22.5	[6]
8	Pd@Peptide	H_2O	K_3PO_4	RT	4	99	16.67	[7]
9	Pd(II)/G1-MNPs	H_2O	Na_2CO_3	80	4	58	14.5	[8]
10	Pd-Fe_3O_4 heterodimer NCs	DME /H_2O	Na_2CO_3	reflux	24	99	4.17	[9]
11	C/Co@PNIPAM-Pd	Toluene/ H_2O	K_2CO_3	85	16	99	2.1	[10]

References:

[1] H. Liu, C.-Y. Cao, F.-F. Wei, Y. Jiang, Y.-B. Sun, P.-P. Huang, W.-G. Song, *J. Phys. Chem. C* **2013**, *117*, 21426.

[2] A. Indra, C. S. Gopinath, S. Bhaduri, G. Kumar Lahiri, *Catal. Sci. Technol.* **2013**, *3*, 1625.

[3] A. Alizadeh, M. M. Khodaei, D. Kordestania, M. Beygzadeh, *Journal of Molecular Catalysis A: Chemical* **2013**, *372*, 167.

[4] X. Huang, Y. Li, Y. Chen, E. Zhou, Y. Xu, H. Zhou, X. Duan, Y. Huang, *Angew. Chem. Int. Ed.* **2013**, *52*, 2520.

[5] R. Li, P. Zhang, Y. Huang, P. Zhang, H. Zhong, Q. Chen, *J. Mater. Chem.* **2012**, *22*, 22750.

[6] Q. Zhang, J. Xu, D. Yan, S. Li, J. Lu, X. Cao, B. Wang, *Catal. Sci. Technol.* **2013**, *3*, 2016.

[7] M. A. Khalily, O. Ustahuseyin, R. Garifullin, R. Genc, M. O. Guler, *Chem. Commun.* **2012**, *48*, 11358.

[8] Y. Liao, L. He, J. Huang, J. Zhang, L. Zhuang, H. Shen, C.-Y. Su, *ACS Applied Materials & Interfaces* **2010**, *2*, 2333.

[9] Y. Jang, J. Chung, S. Kim, S. W. Jun, B. H. Kim, D. W. Lee, B. M. Kim, T. Hyeon, *Phys. Chem. Chem. Phys.* **2011**, *13*, 2512.

[10] M. Zeltner, A. Schatz, M. L. Hefti, W. J. Stark, *J. Mater. Chem.* **2011**, *21*, 2991.